Published in final edited form as:
ChemMedChem. 2016 November 07; 11(21): 2410–2421. doi:10.1002/cmdc.201600417.

Targeting a Targeted Drug: An Approach Toward Hypoxia-Activatable Tyrosine Kinase Inhibitor Prodrugs

Claudia Karnthaler-Benbakka[a], **Diana Groza**[b], **Bettina Koblmüller**[b], **Dr. Alessio Terenzi**[a,c], **Katharina Holste**[b], **Melanie Haider**[b], **Dina Baier**[b], **Prof. Dr. Walter Berger**[b,c], **Dr. Petra Heffeter**[*,b,c], **Dr. Christian R. Kowol**[*,a,c], and **Prof. Dr. Dr. Bernhard K. Keppler**[a,c]

[a]Institute of Inorganic Chemistry, University of Vienna, Waehringer Straße 42, 1090 Wien (Austria)

[b]Institute of Cancer Research and Comprehensive Cancer Center, Medical University of Vienna, Borschkegasse 8A, 1090 Wien (Austria)

[c]Research Platform “Translational Cancer Therapy Research”, University of Vienna and Medical University of Vienna, (Austria)

Abstract

Tyrosine kinase inhibitors (TKIs), which have revolutionized cancer therapy over the past 15 years, are limited in their clinical application due to serious side effects. Therefore, we converted two approved TKIs (sunitinib and erlotinib) into 2-nitroimidazole-based hypoxia-activatable prodrugs. Kinetics studies showed very different stabilities over 24 h; however, fast reductive activation via *E. coli* nitroreductase could be confirmed for both panels. The anticancer activity and signaling inhibition of the compounds against various human cancer cell lines were evaluated in cell culture. These data, together with molecular docking simulations, revealed distinct differences in the impact of structural modifications on drug binding to the enzymes: whereas the catalytic pocket of the epidermal growth factor receptor (EGFR) accepted all new erlotinib derivatives, the vascular endothelial growth factor receptor (VEGFR)-inhibitory potential in the case of the sunitinib prodrugs was dramatically diminished by derivatization. In line, hypoxia dependency of ERK signaling inhibition was observed with the sunitinib prodrugs, while oxygen levels had no impact on the activity of the erlotinib derivatives. Overall, proof of principle could be shown for this concept, and the results obtained are an important basis for the future development of tyrosine kinase inhibitor prodrugs.

Keywords

cancer; hypoxia; prodrugs; targeted therapeutics; tyrosine kinase inhibitors

Introduction

The development of targeted therapies, including small molecule inhibitors and antibodies, has led to a distinct improvement in the treatment of certain forms of cancer during the past

christian.kowol@univie.ac.at, petra.heffeter@meduniwien.ac.at.

Europe PMC Funders Author Manuscripts

one and a half decades. Due to the fact that over 70% of the known oncogenes and proto-oncogenes involved in cancer encode tyrosine kinases (TKs), and the high drugability of this enzyme class, TKs have become the favored therapeutic targets of the pharmaceutical industry.[1] Currently, 25 small molecule tyrosine kinase inhibitors (TKIs), including dual specificity inhibitors, have been approved by the Food and Drug Administration (FDA), half of them in the past five years.[2] With nine drugs targeting the vascular endothelial growth factor receptor (VEGFR) and six the epidermal growth factor receptor (EGFR), these two TKs are among the most extensively used primary targets for kinase inhibition. However, despite the remarkable success in cancer treatment and the belief that these targeted drugs would be much better tolerated than conventional chemotherapeutics, clinical experience revealed unexpected, serious toxic effects.[3] Various organs, such as heart, lungs, liver, kidneys, thyroid and skin, as well as the gastrointestinal tract and nervous system are affected. These side effects are mainly caused by down-stream inhibition of the vascular endothelial growth factor (VEGF) or epidermal growth factor (EGF) signaling in healthy tissues.[3] Thus, a strategy to decrease or circumvent adverse effects would be of high interest, in order to maintain or even increase the upward trend of use and applicability of these drugs.

Strategies to increase the tumor accumulation/specificity in the field of TKIs are so far mainly based on nanoparticle formulations.[1b, 4] Other possibilities, such as the design of inactive prodrugs which are specifically activated in the malignant tissue by exploiting tumor-intrinsic conditions or processes, remain widely unexplored for TKIs.[5] One of these conditions is hypoxia, which was shown to be chronically and/or transiently inherent in most solid tumors. Due to its therapeutic importance, hypoxia evolved as a highly interesting target for cancer therapy and several hypoxia-activatable cytotoxic compounds are already in clinical development.[6] Notably, an important task for the successful application of such prodrugs is the evaluation of tumor hypoxia in patients in order to determine the most effective treatment and predict or monitor response to therapy.[7] To this aim, besides invasive methods, such as pO_2 histography or ex vivo immunohistochemical staining with hypoxia markers (e.g., glucose transporter 1 (GLUT-1) or carbonic anhydrase 9 (CA-IX)), non-invasive imaging technologies, including [^{18}F]fluoromisonidazole ([^{18}F]FMISO) and copper diacetylbis(*N*4-methylthiosemicarbazone) (Cu-ATSM) for positron emission tomography (PET) have been approved.[7, 8] In addition, more recently, several highly innovative approaches using imaging agents for in vivo biomarker detection, for example, enhanced levels of reductive enzymes, have been published.[9] In the future, these new methods could also be useful for verifying the presence and determining the amount of suitable enzymes for prodrug activation.

For prodrug development, we chose the following two TKIs due to their connection to tumor hypoxia: The VEGFR inhibitor sunitinib (Sutent®), which has been approved for the treatment of gastrointestinal stromal tumors (GIST) after failure of imatinib treatment, advanced renal cell carcinoma (RCC), and unresectable or metastatic pancreatic neuroendocrine tumors (pNET); and the EGFR inhibitor erlotinib (Tarceva®), which has been approved for the first-line treatment of locally advanced or metastatic non-small-cell lung cancer (NSCLC) with EGFR-activating mutations, and metastatic pancreatic cancer in combination with gemcitabine.[2b, 10] While it is well known that VEGF gene

overexpression strongly correlates with hypoxia,[11] many tumors that overexpress EGFR, such as NSCLC and pancreatic cancer, also show exceptionally low median tumor oxygen partial pressures.[12]

The aim of this study was to explore the possibility of preparing hypoxia-selective prodrugs of clinically approved VEGFR and EGFR inhibitors. As small structural modifications of these drugs can lead to distinctly reduced kinase inhibition activities, the approved drugs were used for the prodrug design without any additional chemical modifications. As hypoxia-selective functional group, a self-immolative 2-nitroimidazole moiety was used. The combined concepts of TK inhibition and activation by hypoxia should lead to a lower level of the active compound in the non-malignant tissue, and, thus, should increase the therapeutic efficacy while decreasing the adverse effects of the approved compounds.

Results and Discussion

Prodrug design

In general, the prodrug design requires inactivation of the drug by derivatizing a position crucial for its anticancer activity. For a TKI, this is a part of its structure essential for binding to the catalytic pocket of the target kinase. At the same time, the prodrug derivatization should be reversible to ensure the release of the original drug in the tumor tissue. In the case of erlotinib, a crucial nitrogen for prodrug design can be found at the aniline moiety which points toward a hydrophobic region of the adenosine triphosphate (ATP)-binding pocket of the EGFR (Figure 1A). Structure–activity relationship studies revealed that even methylation of this amino function strongly decreases its inhibitory activity.[13] A suitable position for sunitinib derivatization is the oxindole nitrogen, which forms a hydrogen bond to Glu917 in the adenine pocket of the VEGFR (Figure 1B).[14]

As hypoxic trigger the 2-nitroimidazole-5-yl unit was chosen, which was introduced via a carbamate linkage. This moiety has already been shown to undergo hypoxia-selective biochemical reduction in vitro and in vivo and was used in several prodrug systems, including the phosphoramidate mustard prodrug TH-302 (Evofosfamide), which is currently in phase III clinical studies.[6b, 15] The underlying mechanism of the 2-nitroimidazole activation is shown in Scheme 1A. It involves a one-electron reduction by intracellular oxidoreductases, such as the nicotinamide adenine dinucleotide phosphate (NADPH) cytochrome P450 reductase,[6a] to a nitro radical anion, which in the presence of oxygen can efficiently be reoxidized to the parental prodrug. Under hypoxic conditions, however, it is further reduced to the hydroxylamine species, which upon 1,6-elimination releases the active compound. Furthermore, prodrug derivatives with an additional *p*-aminobenzyl self-immolative linker unit were prepared to further increase the steric hindrance of binding the catalytic pocket of the kinase.[16] For these prodrugs, the release of the active drug is expected to be a two-step process: the first step includes the reductive activation of the 2-nitroimidazole, followed by the spontaneous decomposition of the linker via 1,6-elimination with subsequent release of the drug (Scheme 1B).

Synthesis

As core unit for the conjugation of a 2-nitroimidazole moiety to the TKIs, 1-methyl-2-nitro-1*H*-imidazole-5-methanol (**8**) was used. This moiety was synthesized by a modified method from Matteucci et al.[17] in a six-step procedure starting from sarcosine methyl ester hydrochloride (Scheme 2). In contrast with the original literature, methyl formate was used instead of ethyl formate, resulting in changes of reaction conditions and times. This modification was done to avoid transesterification reactions, leading to a product mixture of methyl- and ethyl esters upon ring closure. The synthetic pathway involved *N*- and *C*-formylation of the substrate, followed by ring formation with cyanamide to give the amino ester **5**. Treatment with $NaNO_2$ and HOAc yielded the nitro ester **6**, which was converted into the carboxylic acid **7** by basic hydrolysis. After activation of the acid via mixed acid anhydride, mild reduction with $NaBH_4$ led to **8**.

For conjugation reactions, alcohol **8** was activated with 4-nitrophenyl chloroformate to form the 4-nitrophenyl carbonate **9**. To obtain the self-immolative linker-containing trigger, a 4-aminobenzyl moiety was introduced by condensation of **9** with 4-aminobenzyl alcohol in the presence of HOBt. Further activation of the formed alcohol **10** with bis(4-nitrophenyl) carbonate gave the activated species **11** (Scheme 2).

To synthesize the sunitinib-based prodrugs, commercially available sunitinib was reacted with the active ester **9** for 68 h in the presence of 4-(dimethylamino)pyridine (4-DMAP) yielding **1a**. The same conditions were applied to the linker-containing trigger **11** to form prodrug **1b** (Scheme 3).

Attempts to analogously synthesize the erlotinib-based prodrugs were not successful, as the formed carbamates were not stable enough to isolate the desired products. Thus, a new strategy, involving the alkylation of the NH moiety of erlotinib via an alkyl halide was followed, in order to give a directly linked trigger-(linker)-drug unit. To this end, erlotinib was reacted with the chloride, as well as the bromide derivative of 8, synthesized from the alcohol via $SOCl_2$ or $SOBr_2$, respectively. However, all attempts (*t*BuOK, DMF abs., with/without NaI, 0°C→room temperature→80°C, 18–48 h) failed to give the desired nitroimidazole-erlotinib prodrug. Interestingly, when using 4-nitrobenzyl bromide (in the presence of *t*BuOK) instead of the nitroimidazole bromide, the reaction yielded the desired derivative **2a** (Scheme 4). The synthetic route toward the linker-containing erlotinib prodrug started with the reaction of erlotinib with boc-4-aminobenzyl bromide, followed by deprotection of the amino function using concentrated HCl, giving **2b**. Final condensation with **9** in the presence of HOBt yielded prodrug **2c** (Scheme 4).

Chemical stability and reductive activation via nitroreductase

All synthesized prodrugs were tested for their stability in phos phate buffer (10 mM, pH 7.4) at 37°C, monitored by reversed-phase HPLC chromatography. While the sunitinib-based carbamate prodrugs **1a** and **1b** showed a fast hydrolysis with only 14% and 4% of intact prodrug remaining after 24 h, respectively, the erlotinib-based prodrugs **2a**, and **2c** showed much higher stability with 88% and 76% of remaining substance after the same time, respectively (Supporting Information Figures S11–S15).

To verify whether the prodrugs can be activated and fragmented to the originally active drugs, oxygen-insensitive nitroreductase (NTR) from *E. coli* B was used. This reductase is the most extensively used enzyme for antibody-directed and gene-directed enzyme prodrug therapy (ADEPT and GDEPT) strategies and provides the great advantage that substrates are reduced in a concerted two-electron reduction, bypassing the oxygen-sensitive prodrug radical, which is readily reoxidized to the original prodrug in the presence of oxygen.[18] Thus, the environmental oxygen levels have no impact on the experimental setting. The activation of the prodrugs by NTR reduction was evaluated by incubating aqueous solutions (2.5 μM) of the compounds with NADH (50 μM) and NTR (1.33 μg mL^{-1}) at 37°C. All prodrugs were substrates for NTR and were readily reduced with half-lives of < 6 min and at least 90% conversion of the parent compound after 15 min, showing proof of principle for this strategy (Table 1). For the decay curves of the sunitinib prodrugs **1a** and **1b**, much faster enzymatic activation relative to hydrolysis was observed (substrate remaining after 15 min: 0% for enzymatic activation vs. 78% for hydrolysis in the case of **1a**, and 10% vs. 51% for **1b**). As an example, the release of sunitinib from carbamate **1a** as a function of time is shown in Figure 2.

As desired, after activation, the prodrugs **1a**, **1b**, and **2a** fragmented with release of the unmodified, clinically approved TKI. However, this was not true for **2c**, where the final product could be identified as the amine **2b**, implying a stop of the 1,6-elimination process at the amino position of the 4-aminobenzyl moiety. Notably, not all compounds reached quantitative end points for their corresponding active drug (or amine in the case of **2c**), which is consistent with findings of other groups.[19] This was especially apparent for **1b** and **2a** (58% and 44% respectively), where 4-nitro- or 4-aminobenzyl units were involved.

Establishment of appropriate cell line panels for sunitinib and erlotinib prodrug testing

To select appropriate cell line panels for the biological testing of our prodrug systems, a collection of cell models was tested for their sensitivity toward sunitinib and erlotinib (Table 2). As sunitinib has been approved for the treatment of renal cell carcinoma, several cell lines of this tumor type were included in this panel as well as several cell models with different EGFR status (mutated vs. wild-type and overexpressed). Most of the tested cell models proved to be sensitive toward sunitinib treatment with IC_{50} values < 10 μM. The only exception was Caki-2, which was sunitinib-resistant, while H1703 displayed the highest sensitivity with an IC_{50} value in the high nM range. The sunitinib sensitivity was in agreement with data from western blot analysis performed in parallel (Figure 3), which showed expression of VEGFR-1 in all cell models tested, again with the exception of Caki-2, indicating that this cell line lacks proper target expression. In addition, H1703 displayed an overexpression of the sunitinib target PDGFRβ, which together with the high sunitinib sensitivity demonstrates the dependency of the cells on this signaling pathway.

With regard to erlotinib sensitivity, the data were in agreement with the expectations based on previous reports.[5c, 20] Thus, cell lines harboring an activating EGFR mutation (HCC827 and PC-9) were, together with the EGFR-dependent Calu3 and the wild-type EGFR-overexpressing A431 cell line, the only erlotinib-sensitive models (Table 2). All the other cell lines had IC_{50} values above the solubility limit of erlotinib (25 μM). Interestingly,

the western blots indicated that RU-MH expressed substantial levels of EGFR without being sensitive to erlotinib. This might be based on rather high c-Met expression of this cell line (data not shown), a known resistance factor toward erlotinib.[21]

Biological evaluation of the prodrugs in long- and short-term treatment

As a first approach, we analyzed the prodrug nature as well as the impact of oxygen levels on the anticancer activity of our novel drugs in 72 h viability assays (Table 3 and Table 4). As reference compounds, unmodified sunitinib and erlotinib were used. In addition, the phosphoramidate mustard prodrug TH-302 (Evofosfamide), which is currently in phase III clinical studies[6b, 15c] and also contains a 2-nitroimidazole-5-yl unit as hypoxic trigger, was included as a positive control for activation under hypoxic conditions (Table 5). As already expected from the low stability of our prodrugs in the reversed-phase HPLC chromatography experiments described above, no significant difference in the activity was found between hypoxic and normoxic conditions and **1a** and **1b** behaved widely similar to sunitinib (Table 3). Also **2a** and **2b**, while being less active than erlotinib, followed the pattern of the EGFR inhibitor, with highest activity in the erlotinib-hypersensitive HCC827 and PC-9 models (Table 4). In contrast, **2c** did not show an EGFR-dependent activity pattern with the lowest IC_{50} value in the erlotinib-nonresponsive MCF-7 and the highest IC_{50} values in erlotinib-hypersensitive PC-9 and Calu3 cells. In line with these data, preliminary results using HCC827/ER cells, which have been selected for erlotinib resistance (based on c-Met overexpression), displayed significant sensitivity toward **2c** but not **2a** and **2b**, which overall suggests that this derivative has cytotoxic potential independent from EGFR inhibition (data not shown).

Due to the low drug stability of **1a** and **1b**, the 72 h viability assays turned out to not be suitable for proof of concept studies of our prodrugs. Therefore, short-term (4 h) experiments with inhibition of the TK signaling (phosphorylation of ERK) as a read out were performed. Figure 4A shows that indeed, especially in case of **1a**, decreased inhibition of ERK phosphorylation (relative to sunitinib) under normoxic conditions was observed. In contrast, an activity similar to free sunitinib was found under hypoxia. With regard to the erlotinib prodrugs, no difference between erlotinib and **2c** (Figure 4B) or **2a** (data not shown) were found with respect to oxygen levels.

Molecular docking

To understand the biological results and investigate whether the sunitinib and erlotinib derivatives **1a**, **1b**, and **2a–c** are able to enter the VEGFR- and EGFR-binding pockets in their prodrug form, molecular docking simulations were performed using AutoDock Vina. PDB ID: 4AGD and PDB ID: 1M17 were used as models for VEGFR-2 and EGFR, respectively.

Sunitinib, as previously mentioned and as shown by the 2D plot in Supporting Information Figure S21, is located in the ATP-binding pocket of VEGFR-2, forming a hydrogen bond to Glu917, as well as a hydrogen bond with Asn923 with a water molecule acting as bridge. Our calculations showed that, in contrast to sunitinib, both **1a** and **1b**, did not fit into the binding pocket in any of the possible poses (Figure 5 and Figure S21, representing the 3D

and 2D plots of the best poses, respectively). This is in agreement with the experimental results as, despite their instability, **1a** and **1b** have potential to act as sunitinib prodrugs.

Surprisingly, the erlotinib derivatives **2a–c** retained the ability to enter the EGFR ATP-binding pocket, regardless of their steric hindrance. The 2D schematic diagrams of protein-ligand interactions in Figure 6 show that the nitrogen of the quinazoline core in **2a** and **2c** still accepts the hydrogen bond from the Met769 amide nitrogen, as the unmodified erlotinib does. Compound **2b** can also be placed in the binding pocket with the other quinazoline nitrogen atom retaining its hydrogen bond with the Thr766 side chain via a water molecule bridging the gap in distance, as for erlotinib. 3D cartoons in Figure 7 emphasize the ability of the quinazoline core of **2a–c** to fit exactly in the catalytic cleft of EGFR. Interestingly, compound **2c** uses its nitroimidazole side chain as an arm to stabilize the interaction of the quinazoline core inside the protein binding pocket (Figure 6C and 7A). Overall, these results may explain the biological activity of compounds **2a–c** as they are able to act as erlotinib-type drugs rather than erlotinib prodrugs.

Conclusions

With the aim of generating prodrugs of targeted therapeutics, we synthesized a series of potentially hypoxia-activatable 2-nitroimidazole derivatives of the TKIs sunitinib and erlotinib. In cell-free experiments, these compounds were readily activated by NTR, delivering proof of principle for this strategy. However, the sunitinib prodrugs **1a** and **1b** were highly labile in aqueous solution, and the erlotinib derivative **2c** revealed fragmentation products other than the original drug. For biological testing, appropriate cell line panels were established. However, 72 h drug treatment followed by cell viability analyses revealed no difference in the activity between the prodrugs and their corresponding free drugs independent of the oxygen level. The reasons are, on the one hand, the compound lability (**1a** and **1b**) and, on the other hand, preserved enzyme inhibition (**2a–c**), as suggested by docking simulations. The latter disclosed distinct differences in the impact of structural modifications on the drug interaction with the ATP-binding pocket of the respective enzymes. Notably, **2c** showed unexpected behavior with potent EGFR-independent activity, indicating an additional mechanism of action, which will be the topic of further investigations. Interestingly, **1a** and **1b**, however, despite their applicability-limiting instability, still proved to be sunitinib prodrugs also in vitro. This was verified by short-term incubation experiments, where some hypoxia dependency of ERK signaling inhibition was observed especially in the case of the more stable **1a**.

In general, TKIs are appealing drug candidates for prodrug design, as their adverse effects lead to limitations in the clinical application. Furthermore, from the chemical point of view, their mechanism of action involves selective enzyme binding, which can be prevented by specific derivatization. However, in contrast to common cytotoxic drugs, such as doxorubicin or paclitaxel, which comprise primary amino or hydroxy groups that can be easily functionalized resulting in stable prodrugs, in the case of TKIs, derivatization is a very complex issue. In the panel of clinically approved TKIs, hardly any chemically easily accessible group can be found in a crucial position. Thus, based on the results of our study, we conclude that a compromise has to be found between prodrug stability and the guarantee

Europe PMC Funders Author Manuscripts

of release of the approved original drug. Moreover, careful considerations have to be made regarding the design of such derivatives, because the very heterogeneous enzyme targets of these drugs show distinct differences in enzyme tolerability for structural modifications on the drugs. Thus, the development of an optimized prodrug requires the validation of a TKI with a suitable crucial functionality meeting all of these requirements, which is currently in progress in our group.

Experimental Section

Chemistry

All solvents and reagents were obtained from commercial suppliers and used without further purification. Anhydrous solvents were bought over molecular sieves from Fisher Scientific (Austria) GmbH. Erlotinib and sunitinib were purchased from LC Laboratories®, sarcosine methyl ester hydrochloride from Alfa Aesar. Mass spectrometry was performed on a Bruker HCT plus ESI-QIT spectrometer and high resolution spectra were obtained from a Bruker maXis ESI-Qq-oaRTOF spectrometer. Expected and experimental isotope distributions were compared. ^{1}H and ^{13}C NMR spectra were recorded in [D_6]DMSO with a Bruker Avance III 500 MHz spectrometer at 500.32 (^{1}H) and 125.81 (^{13}C) MHz at 298 K, with chemical shifts referenced to the solvent residual peak as an internal standard. NMR data are reported indicating the chemical shift (δ, (ppm)), the multiplicity (s, singlet; d, doublet; t, triplet; q, quartet; m, multiplet, etc.), the coupling constant (J, (Hz)), and the integration. Assignments of the ^{1}H and ^{13}C shifts of **1a**, **1b**, and **2a–2c** were carried out according to the atom numberings shown in the Supporting Information Figures S1–S10. All final compounds displayed ≥ 95% purity as determined by elemental analysis performed by the Microanalytical Laboratory of the University of Vienna. Stability and reductive activation were determined by RP-HPLC on a Dionex UltiMate 3000 UHPLC system controlled by Chromeleon 6.8 chromatography software. The experimental conditions were as follows: stationary phase: ethylene bridged hybrid C_{18}; column: Acquity UPLC BEH C_{18}, 130 Å, 1.7 μm, 3.0 mm × 50 mm (Waters Corp.); column temperature: 25°C; mobile phase: H_2O/MeCN (0.1% HCOOH), HPLC grade; flow rate: 0.6 $mLmin^{-1}$, injection volume: 10 μL; gradient: 5–95% MeCN in 6 min. Decomposition products were identified via HPLC–MS on a 1260 Infinity Bio-Inert LC System from Agilent Technologies, controlled by an Agilent OpenLAB CDS ChemStation software (Edition Rev. C.01.06), coupled to an amaZon SL Ion Trap mass spectrometer with HyStar 3.2 and Data Analysis 4.0 software package (Bruker Daltonics).

Methyl *N*-formyl-*N*-methylglycinate (3)—This compound and all following synthetic steps until compound **8** were synthesized by a modified procedure from Matteucci et al.,[17] using methyl formate instead of ethyl formate. Sarcosine methyl ester hydrochloride (25 g, 180 mmol) in MeOH (100 mL) was treated with methyl formate (77.3 mL, 7.0 equiv) and K_2CO_3 (49.8 g, 2.0 equiv) and stirred for 26 h. The formed precipitate was filtered off and washed with MeOH. The filtrate was concentrated, diluted with H_2O (65 mL) and extracted with CH_2Cl_2 (4×50 mL). The combined organic phases were dried over Na_2SO_4, filtered, and concentrated to give **3** as a colorless oil (12.62 g, 54%): ^{1}H NMR (500.32 MHz,

[D_6]DMSO): two rotamers: δ = 2.76 (s, 3H), 2.97 (s, 3H), 3.67 (s, 3H), 3.70 (s, 3H), 4.07 (s, 2H), 4.22 (s, 2H), 8.02 (s, 1H), 8.10 ppm (s, 1H).

Sodium 3-methoxy-2-(*N*-methylformamido)-3-oxoprop-1-en-1-olate (4)— Compound **3** (8.3 g, 63 mmol) in methyl formate (13.7 mL, 3.5 equiv) was added dropwise to an ice cold mixture of NaOMe (3.76 g, 1.1 equiv) in dry THF (30 mL) over a period of 1.5 h. The mixture was allowed to slowly warm to ambient temperature. After 23 h, it was treated with Et_2O (30 mL) and the resulting white powder (**4**) was filtered off and washed with Et_2O (9.01 g, 79%): ^{1}H NMR (500.32 MHz, [D_6]DMSO): δ = 2.70 (s, 3H), 3.44 (s, 3H), 7.56 (s, 1H), 8.92 ppm (s, 1H).

2-Amino-1-methyl-1*H*-imidazole-5-carboxylic acid methyl ester (5)—A stirred solution of **4** (10.39 g, 57.37 mmol) in MeOH (100 mL) and 30% HCl (14.3 mL, 2.35 equiv) was heated at 110°C and stirred for 23 h. Then, the reaction mixture was cooled to ambient temperature and filtered. The residue was washed with MeOH and the combined filtrates concentrated to yield a brown oil, which was diluted with 10% HOAc (63.5 mL), NH_2CN (5.30 g, 2.2 equiv) and NaOAc (10.35 g, 2.2 equiv) and stirred for 3 h at 100°C. The reaction mixture was cooled down, concentrated to half of its volume, and the solution was adjusted to pH ~ 9 by the addition of a saturated K_2CO_3 solution. The resulting mixture was extracted with EtOAc (8×100 mL), and the organic phases were concentrated in vacuo. The crude product was purified by flash chromatography on silica gel, eluting with EtOAc/MeOH 9:1, to give **5** as a white powder (2.46 g, 28%): ^{1}H NMR (500.32 MHz, [D_6]DMSO): δ = 3.53 (s, 3H), 3.69 (s, 3H), 6.20 (s, 2H), 7.30 ppm (s, 1H).

1-Methyl-2-nitro-1*H*-imidazole-5-carboxylic acid methyl ester (6)—Compound **5** (563 mg, 3.63 mmol) in HOAc (3.4 mL) was added dropwise to an ice-cold solution of $NaNO_2$ (1.67 g, 6.65 equiv) in H_2O (5 mL) over a period of 1 h. The temperature was slowly raised to ambient temperature. After 22 h the solution was extracted with CH_2Cl_2 (3×6 mL), the combined organic phases were dried over Na_2SO_4, filtered, and concentrated. The crude product was purified by flash chromatography on silica gel, eluting with EtOAc/hexane 7:3, to give **6** as light-yellow powder (390 mg, 58%): ^{1}H NMR (500.32 MHz, [D_6]DMSO): δ = 3.89 (s, 3H), 4.20 (s, 3H), 7.81 ppm (s, 1H).

1-Methyl-2-nitro-1*H*-imidazole-5-carboxylic acid (7)—To a stirred solution of **6** (390 mg, 2.11 mmol) in H_2O (2 mL), NaOH (1 M, 6.5 mL) was added and the mixture was stirred for 20 h at room temperature. The resulting solution was acidified with conc. HCl to pH 1 and extracted with EtOAc (5×6.5 mL). The combined organic phases were dried over $MgSO_4$, filtered, and concentrated to give **7** as a pale-yellow powder (1.1 g, 89%): ^{1}H NMR (500.32 MHz, [D_6]DMSO): δ = 4.20 (s, 3H), 7.75 (s, 1H), 13.90 ppm (s, 1H).

1-Methyl-2-nitro-1*H*-imidazole-5-methanol (8)—To a stirred solution of 7 (1.08 g, 6.31 mmol) and Et_3N (1.4 mL, 1.6 equiv) in dry THF (28 mL) isobutyl chloroformate (1.31 mL, 1.6 equiv) was added dropwise over a period of 10 min at −60°C. The reaction mixture was stirred for 2 h and then treated with $NaBH_4$ (1.25 g, 5.25 equiv) at −15°C. After 10 min, H_2O (26 mL) was added over a period of 1 h while maintaining the temperature between

−10°C and 0°C. After raising the temperature to 5°C, the solid was filtered off, washed with THF, and the combined THF portions were concentrated. The crude product was diluted with HCl (0.1 M, 35 mL), acidified to pH 3 with HCl (1 M) and extracted with EtOAc (9×17 mL). The combined organic phases were dried over Na_2SO_4, filtered, and concentrated in vacuo to give **8** as light-yellow powder (886 mg, 89%): ^{1}H NMR (500.32 MHz, [D$_6$]DMSO): δ = 3.93 (s, 3H), 4.55 (s, 2H), 5.56 (s, 1H), 7.12 ppm (s, 1H); ^{13}C NMR (125.81 MHz, [D$_6$]DMSO): δ = 34.6, 53.5, 127.0, 139.1, 146.2 ppm; MS (ESI) *m*/*z*: 180.18 [*M* + Na]$^+$.

(1-Methyl-2-nitro-1*H*-imidazol-5-yl)methyl (4-nitrophenyl) carbonate (9)—To an ice-cold solution of 4-nitrophenyl chloroformate (770 mg, 3.82 mmol, 1.5 equiv) in dry THF (30 mL), pyridine (308 μL, 1.5 equiv) was slowly added. After 30 min at 0°C, **8** (400 mg, 2.55 mmol, 1 equiv) dissolved in dry THF (10 mL) was added dropwise for 10 min. After another 10 min at 0°C, the reaction mixture was allowed to warm to ambient temperature and was stirred for 20 h. CH_2Cl_2 (40 mL) was added and the mixture was washed with HCl (1 M, 3×40 mL) and brine (30 mL). The combined organic layers were dried over $MgSO_4$, filtered, and concentrated in vacuo. The crude product was purified by recrystallization from EtOAc/hexane to give the product as beige crystals (486 mg, 59%): ^{1}H NMR (500.32 MHz, [D$_6$]DMSO): δ = 3.99 (s, 3H), 5.47 (s, 2H), 7.37 (s, 1H), 7.60 (d, *J* = 9 Hz, 2H), 8.34 ppm (d, *J* = 9 Hz, 2H); ^{13}C NMR (125.81 MHz, [D$_6$]DMSO): δ = 34.8, 59.9, 123.1, 125.9, 130.1, 131.9, 145.8, 146.8, 151.9, 155.6 ppm; MS (ESI) *m*/*z*: 345.16 [*M* + Na]$^+$.

(1-Methyl-2-nitro-1*H*-imidazol-5-yl)methyl (4-(hydroxymethyl)-phenyl)carbamate (10)—To a mixture of HOBt·H_2O (203 mg, 1.50 mmol), molecular sieve 4 Å (250 mg), and 4-aminobenzyl alcohol (278 mg, 1.5 equiv) in dry DMF (5 mL), **9** (485 mg, 1 equiv) was added and the resulting reaction mixture was stirred for 18 h at room temperature. The molecular sieve was filtered off and the solvent was removed. The crude product was purified by flash chromatography on silica gel, eluting with EtOAc/Hexane 2:1, to give **10** as a white powder (370 mg, 80%): ^{1}H NMR (500.32 MHz, [D$_6$]DMSO): δ = 3.98 (s, 3H), 4.42 (d, *J* = 6 Hz, 2H), 5.09 (t, *J* = 6 Hz, 1H), 5.29 (s, 2H), 7.23 (d, *J* = 8 Hz, 2H), 7.32 (s, 1H), 7.41 (d, *J* = 8 Hz, 2H), 9.79 ppm (s, 1H).

(1-Methyl-2-nitro-1*H*-imidazol-5-yl) methyl (4-((((4-nitrophenoxy)carbonyl)oxy)methyl)phenyl) carbamate (11)—A solution of **10** (206 mg, 0.673 mmol) and DIPEA (352.4 μL, 3 equiv) in dry DMF (15 mL) was treated with bis(4-nitrophenyl) carbonate (307 mg, 1.5 equiv), and the reaction mixture was stirred at room temperature for 25 h. Then, EtOAc (170 mL) was added and the organic layer was washed with KOH (0.01 M, 12×40 mL) and brine (1×40 mL), dried over $MgSO_4$, filtered, and concentrated in vacuo to give **11** as a beige solid (271 mg, 85%): ^{1}H NMR (500.32 MHz, [D$_6$]DMSO): δ = 3.99 (s, 3H), 5.24 (s, 2H), 5.31 (s, 2H), 7.33 (s, 1H), 7.42 (d, *J* = 9 Hz, 2H), 7.51 (d, *J* = 9 Hz, 2H), 7.58 (d, *J* = 9 Hz, 2H), 8.33 (d, *J* = 9 Hz, 2H), 9.97 ppm (s, 1H).

(1-Methyl-2-nitro-1*H*-imidazol-5-yl)methyl (*Z*)-3-((4-((2-(diethylamino)ethyl)carbamoyl)-3,5-dimethyl-1*H*-pyrrol-2-yl)methylene)-5-

fluoro-2-oxoindoline-1-carboxylate (1 a)—Sunitinib (155 mg, 0.390 mmol) was added to a solution of **9** (151 mg, 1.2 equiv) and 4-dimethylaminopyridine (57 mg, 1.2 equiv) in dry THF (15 mL), which had been stirred for 5 min. The resulting reaction mixture was stirred for 68 h in the dark. H_2O (15 mL) was added and the mixture was stored at 4°C for 2.5 h. The precipitate was filtered off and washed with THF/H_2O 1:1 and then with H_2O to give **1a** as an orange powder (146 mg, 64%): ^{1}H NMR (500.32 MHz, [D_6]DMSO): δ = 0.98 (t, J = 7 Hz, 6H, H28, H29), 2.45 (s, 3H, H18), 2.48 (s, 3H, H19), 2.49–2.56 (m, 6H, H24, H26, H27), 3.29 (dt, J = 6 Hz, J = 6 Hz, 2H, H23), 4.06 (s, 3H, H40), 5.59 (s, 2H, H33), 7.06 (ddd, ^3J = 9 Hz, $^3J_{HF}$ = 9 Hz, ^4J = 3 Hz, 1H, H2), 7.41 (s, 1H, H35), 7.60 (t, J = 5 Hz, 1H, H22), 7.75–7.77 (m, 2H, H3, H12), 7.93 (dd, $^3J_{HF}$ = 9 Hz, ^4J = 3 Hz, 1H, H6), 12.73 ppm (s, 1H, H14); ^{13}C NMR (125.81 MHz, [D_6]DMSO): δ = 11.1 (C18), 12.3 (C28, C29), 13.9 (C19), 35.0 (C40), 37.5 (C23), 47.0 (C26, C27), 52.1 (C24), 58.0 (C33), 105.9 (C6, $^2J_{CF}$ = 26 Hz), 111.1 (C9, $^4J_{CF}$ = 3 Hz), 113.1 (C2, $^2J_{CF}$ = 24 Hz), 116.2 (C3, $^3J_{CF}$ = 9 Hz), 122.4 (C16), 126.3 (C13), 126.7 (C12), 128.1 (C5, $^3J_{CF}$ = 10 Hz), 129.8 (C35), 131.6 (C4), 132.6 (C34), 133.8 (C17), 139.4 (C15), 146.8 (C37), 150.3 (C30), 160.1 (C1, $^1J_{CF}$ = 239 Hz), 164.5 (C20), 166.7 ppm (C8); MS (ESI) m/z: 582.42 [M + H]$^+$; Anal. calcd for $C_{28}H_{32}FN_7O_6$·0.1 H_2O (M_r = 583.40 g mol^{-1}): C 57.65, H 5.56, N 16.81, found: C 57.40, H 5.40, N, 16.73.

4-((((1-methyl-2-nitro-1*H*-imidazol-5-yl)methoxy)carbonyl)amino)benzyl (*Z*)-3-((4-((2-(diethylamino)ethyl)carbamoyl)-3,5-dimethyl-1*H*-pyrrol-2-yl)methylene)-5-fluoro-2-oxoindoline-1-carboxylate (1 b)—Sunitinib (191 mg, 0.479 mmol) was added to a solution of **11** (271 mg, 1.2 equiv) and 4-dimethylaminopyridine (70.2 mg, 1.2 equiv) in dry THF (8 mL), which had been stirred for 5 min. The resulting reaction mixture was stirred for 69 h in the dark. H_2O (8 mL) was added and the mixture was stored at 4°C for 2 h. The precipitate was filtered off and washed with THF/H_2O 1:1 and then with H_2O to give **1b** as an orange powder (236 mg, 66%): ^{1}H NMR (500.32 MHz, [D_6]DMSO): δ = 0.98 (t, J = 7 Hz, 6H, H28, H29), 2.45 (s, 3H, H18), 2.48 (s, 3H, H19), 2.49–2.55 (m, 6H, H24, H26, H27), 3.29 (dt, J = 6 Hz, J = 6 Hz, 2H, H23), 3.97 (s, 3H, H38), 5.30 (s, 2H, H36), 5.39 (s, 2H, H48), 7.04 (ddd, ^3J = 9 Hz, $^3J_{HF}$ = 9 Hz, ^4J = 3 Hz, 1H, H2), 7.32 (s, 1H, H31), 7.47–7.52 (m, 4H, H43, H44, H46, H47), 7.60 (t, J = 5 Hz, 1H, H22), 7.74 (dd, ^3J = 9 Hz, $^4J_{HF}$ = 5 Hz, 1H, H3), 7.77 (s, 1H, H12), 7.92 (dd, $^3J_{HF}$ = 9 Hz, ^4J = 2 Hz, 1H, H6), 9.98 (s, 1H, H40), 12.73 ppm (s, 1H, H14); ^{13}C NMR (125.81 MHz, [D_6]DMSO): δ = 11.1 (C18), 12.4 (C28, C29), 13.8 (C19), 34.8 (C38), 37.5 (C23), 47.0 (C26, C27), 52.1 (C24), 55.7 (C36), 68.4 (C48), 105.9 (C6, $^2J_{CF}$ = 26 Hz), 111.3 (C9, $^4J_{CF}$ = 3 Hz), 113.0 (C2, $^2J_{CF}$ = 24 Hz), 116.1 (C3, $^3J_{CF}$ = 8 Hz), 118.6 (C43, C47), 122.4 (C16), 126.3 (C13), 126.6 (C12), 128.0 (C5, $^3J_{CF}$ = 10 Hz), 129.3 (C31), 129.9 (C44, C46), 129.9 (C45 or C42), 131.8 (C4), 133.6 (C17), 133.7 (C30), 139.3 (C15), 139.4 (C42 or C45), 146.6 (C33), 150.8 (C50), 153.2 (C39), 160.0 (C1, $^1J_{CF}$ = 239 Hz), 164.6 (C20), 166.8 ppm (C8); MS (ESI) m/z: 731.48 [M + H]$^+$; Anal. calcd for $C_{36}H_{39}FN_8O_8$·0.75 H_2O (M_r = 744.25 gmol^{-1}): C 58.10, H 5.48, N 15.06, found: C 58.38, H 5.43, N 14.70.

***N*-(3-ethynylphenyl)-6,7-bis(2-methoxyethoxy)-*N*-(4-nitrobenzyl)-quinazolin-4-amine (2 a)—**Erlotinib (200 mg, 0.508 mmol) was added to an ice-cold solution of *t*BuOK (63 mg, 1.1 equiv) in dry DMF (10 mL) and stirred for 10 min at 0°C. Then, 4-nitrobenzyl

bromide (143 mg, 1.3 equiv) was added and the reaction mixture was allowed to slowly warm to room temperature and stirred overnight. After 18 h, the solvent was evaporated, the residue was diluted with H_2O (10 mL) and extracted with EtOAc (2×15 mL). The combined organic phases were dried over $MgSO_4$, filtered and concentrated. Purification of the crude product was performed by flash chromatography on silica gel, eluting with EtOAc/MeOH 20:1, to give **2a** as beige crystals (62 mg, 23%): ^{1}H NMR (500.32 MHz, [D_6]DMSO): δ = 3.25 (s, 3H, H29), 3.32 (s, 3H, H25), 3.39–3.41 (m, 2H, H27), 3.55–3.57 (m, 2H, H26), 3.70–3.72 (m, 2H, H23), 4.25 (s, 1H, H19), 4.25–4.27 (m, 2H, H22), 5.55 (s, 2H, H30), 6.46 (s, 1H, H6), 7.26 (s, 1H, H3), 7.28 (ddd, ^3J = 8 Hz, ^4J = 2 Hz, ^4J = 1 Hz, 1H, H17), 7.31 (ddd, ^3J = 8 Hz, ^4J = 1 Hz, ^4J = 1 Hz, 1H, H15), 7.38 (dd, J = 8 Hz, J = 8 Hz, 1H, H16), 7.40 (dd, ^4J = 2 Hz, ^4J = 1 Hz, 1H, H13), 7.69 (d, J = 9 Hz, 2H, H32, H36), 8.15 (d, J = 9 Hz, 2H, H33, H35), 8.66 ppm (s, 1H, H8); ^{13}C NMR (125.81 MHz, [D_6]DMSO): δ = 55.4 (C30), 58.7 (C29), 58.8 (C25), 67.7 (C26), 68.5 (C22), 70.0 (C27), 70.4 (C23), 82.3 (C19), 83.1 (C18), 106.1 (C6), 108.6 (C3), 110.6 (C5), 123.7 (C14), 123.9 (C33, C35), 126.5 (C17), 128.4 (C13), 129.3 (C32, C36), 129.3 (C15), 130.7 (C16), 146.8 (C12), 146.9 (C31), 147.0 (C34), 147.1 (C1), 149.5 (C4), 153.2 (C8), 153.9 (C2), 159.7 ppm (C10); MS (ESI) m/z: 529.40 $[M + H]^+$, 551.35 $[M + Na]^+$; Anal. calcd for $C_{29}H_{28}N_4O_6 \cdot 0.1\ H_2O$ (M_r = 530.36 $gmol^{-1}$): C 65.67, H 5.36, N 10.56, found: C 65.42, H 5.20, N 10.42.

***tert*-butyl (4-(((6,7-bis(2-methoxyethoxy)quinazolin-4-yl) (3-ethynylphenyl)amino)methyl)phenyl) carbamate (12)—**Erlotinib (500 mg, 1.27 mmol) was added to an ice-cold solution of *t*BuOK (185 mg, 1.3 equiv) in dry DMF (25 mL) and stirred for 10 min at 0°C. Then, boc-4-aminobenzyl bromide (473 mg, 1.3 equiv) was added and the reaction mixture was allowed to slowly warm to ambient temperature and stirred overnight. After 20 h the solvent was evaporated, the residue was dissolved in EtOAc (50 mL) and washed with H_2O and brine (25 mL each). The organic phase was dried over Na_2SO_4, filtered, and concentrated. Purification of the crude product was performed by flash chromatography on silica gel, eluting with EtOAc/MeOH 20:1, to give **12** as pale-yellow powder (263 mg, 35%): ^{1}H NMR (500.32 MHz, [D_6]DMSO): δ = 1.45 (s, 9H), 3.25 (s, 3H), 3.32 (s, 3H), 3.39–3.41 (m, 2H), 3.54–3.56 (m, 2H), 3.70–3.72 (m, 2H), 4.21 (s, 1H), 4.25–4.27 (m, 2H), 5.35 (s, 2H), 6.46 (s, 1H), 7.17 (ddd, ^3J = 8 Hz, ^4J = 2 Hz, ^4J = 1 Hz, 1H), 7.24 (s, 1H), 7.26–7.36 (m, 7H), 8.68 (s, 1H), 9.26 ppm (s, 1H); MS (ESI) m/z: 599.47 $[M + H]^+$.

***N*-(4-aminobenzyl)-*N*-(3-ethynylphenyl)-6,7-bis(2-methoxyethoxy)quinazolin-4-amine (2b)—**A stirred solution of 12 (263 mg, 0.439 mmol) in MeOH (20 mL) was treated with HCl conc. (183 μL, 2.2 mmol). After 20 h, the solvent was evaporated to yield the product as a pale-yellow foam (240 mg, 96%). To remove the HCl salt, portions of the product were diluted with $NaHCO_3$ (0.25 M) and extracted with EtOAc. The combined organic phases were dried over Na_2SO_4, filtered, and concentrated. Because some erlotinib was found in the product, it was purified twice by flash chromatography on silica gel (hexane/THF 1:2, followed by CH_2Cl_2/MeOH 20:1 + Et_3N (0.1%)) to give pure **2b** as a beige solid: ^{1}H NMR (500.32 MHz, [D_6]DMSO): δ = 3.24 (s, 3H, H29), 3.32 (s, 3H, H25), 3.39–3.41 (m, 2H, H27), 3.52–3.54 (m, 2H, H26), 3.70–3.72 (m, 2H, H23), 4.19 (s, 1H, H19), 4.24–4.26 (m, 2H, H22), 4.94 (s, 2H, H37), 5.23 (s, 2H, H30), 6.43 (s, 1H, H6), 6.44 (d, J = 8 Hz, 2H, H33, H35), 7.03 (d, J = 8 Hz, 2H, H32, H36), 7.13 (ddd, ^3J = 8 Hz, ^4J = 2

Hz, ^4J = 1 Hz, 1H, H17), 7.20 (dd, ^4J = 2 Hz, ^4J = 1 Hz, 1H, H13), 7.22 (s, 1H, H3), 7.27 (ddd, ^3J = 8 Hz, ^4J = 1 Hz, ^4J = 1 Hz, 1H, H15), 7.34 (dd, J = 8 Hz, J = 8 Hz, 1H, H16), 8.68 ppm (s, 1H, H8); ^{13}C NMR (125.81 MHz, [D$_6$]DMSO): δ = 55.4 (C30), 58.7 (C29), 58.7 (C25), 67.7 (C26), 68.5 (C22), 70.0 (C27), 70.4 (C23), 82.0 (C19), 83.2 (C18), 106.4 (C6), 108.5 (C3), 110.8 (C5), 114.2 (C33, C35), 123.4 (C14), 125.1 (C31), 126.7 (C17), 128.6 (C13), 128.9 (C15), 129.4 (C32, C36), 130.5 (C16), 146.9 (C1), 147.2 (C2), 148.1 (C34), 149.4 (C4), 153.3 (C8), 153.7 (C2), 160.1 ppm (C10); MS (ESI) m/z: 499.36 [M + H]$^+$, 521.40 [M + Na]$^+$, 537.38 [M + K]$^+$; Anal. calcd for $C_{29}H_{30}N_4O_4$·0.25 H_2O (M_r = 503.08 g mol^{-1}): C 69.22, H 6.11, N 11.14, found: C 68.95, H 5.93, N 11.05.

(1-Methyl-2-nitro-1*H*-imidazol-5-yl)methyl (4-(((6,7-bis(2-methoxyethoxy)quinazolin-4-yl) (3-ethynylphenyl)amino)methyl)phenyl) carbamate (2 c)—Compound **2b** (80 mg, 0.16 mmol, 1.1 equiv) was dissolved in dry DMF (6.5 mL) and treated with **9** (47 mg, 0.15 mmol, 1 equiv) and HOBt·H_2O (22 mg, 1.1 equiv). The resulting reaction mixture was stirred overnight at room temperature. After 18 h, it was diluted with brine (30 mL) and extracted with EtOAc (3×25 mL). The combined organic phases were dried over $MgSO_4$, filtered, and concentrated. The crude product was purified by flash chromatography on silica gel, eluting with hexane/THF 1:2, to give **2c** as a pale-yellow powder (83 mg, 77%): ^{1}H NMR (500.32 MHz, [D$_6$]DMSO): δ = 3.24 (s, 3H, H29), 3.31 (s, 3H, H25), 3.38–3.40 (m, 2H, H27), 3.53–3.55 (m, 2H, H26), 3.69–3.71 (m, 2H, H23), 3.95 (s, 3H, H48), 4.23 (s, 1H, H19), 4.24–4.26 (m, 2H, H22), 5.26 (s, 2H, H41), 5.35 (s, 2H, H30), 6.44 (s, 1H, H6), 7.18 (ddd, ^3J = 8 Hz, ^4J = 2 Hz, ^4J = 1 Hz, 1H, H17), 7.23 (s, 1H, H3), 7.26–7.36 (m, 8H, H13, H15, H16, H32, H33, H35, H36, H42), 8.66 (s, 1H, H8), 9.80 ppm (s, 1H, H37); ^{13}C NMR (125.81 MHz, [D$_6$]DMSO): δ = 34.7 (C48), 55.2 (C30), 55.6 (C41), 58.7 (C29), 58.7 (C25), 67.6 (C26), 68.5 (C22), 70.0 (C27), 70.4 (C23), 82.1 (C19), 83.2 (C18), 106.2 (C6), 108.5 (C3), 110.7 (C5), 118.6 (C33, C35), 123.5 (C14), 126.6 (C17), 128.4 (C13), 128.9 (C32, C36), 129.0 (C15), 129.3 (C42), 130.6 (C16), 132.7 (C31), 133.8 (C46), 138.0 (C34), 146.5 (C44), 147.0 (C1), 147.0 (C12), 149.4 (C4), 153.1 (C38), 153.3 (C8), 153.7 (C2), 160.0 ppm (C10); MS (ESI) m/z: 682.26 [M + H]$^+$; Anal. calcd for $C_{35}H_{35}N_7O_8$·0.5 EtOAc·0.5 H_2O (M_r = 734.76 g mol^{-1}): C 60.48, H 5.49, N 13.34, found: C 60.69, H 5.48, N 13.42.

Stability measurements in aqueous buffer

Compounds **1a**, **1b** and **2a–c** were dissolved in sodium phosphate buffer (10 mM, pH 7.4, 37°C) containing 1% DMSO at a concentration of 2.5 μm and incubated at 37°C. Aliquots were withdrawn at different time points (0–24 h, every 30 min) and subjected to RP-HPLC analysis. The HPLC chromatogram peak areas at 420 nm (for **1a**, **1b**) and 340 nm (for **2a–c**) were used to calculate the concentration of the remaining prodrug.

E. coli nitroreductase assay

Recombinant *E. coli* nitroreductase and β-nicotinamide adenine dinucleotide (β-NADH, reduced form, dipotassium salt) were purchased from Sigma–Aldrich. The following protocol was applied to the test compounds: compound stock solution (15 μL, 250 μM) in DMSO was added to sodium phosphate buffer (410 μL, 10 mM, pH 7, preheated to 37°C) and NADH (75 μL of 1 mM) in sodium phosphate buffer. The reaction was initiated by

addition of *E. coli* nitroreductase (1 mL, 2 μg mL^{-1} in sodium phosphate buffer; final concentrations: drug: 2.5 μM; NADH: 50 μM). Aliquots were collected and the reactions were followed by RP-HPLC as a function of time. The HPLC chromatogram peak areas at 420 nm (for **1a**, **1b**) and 340 nm (for **2 a–c**) were used to determine both the disappearance of the starting material as well as the appearance of the reaction products. Unknown peaks were identified using mass spectrometry. Between the time points, all solutions were incubated at 37°C. Reference solutions containing compound stock solution (15 μL) in DMSO, buffer solution (1.410 mL), and NADH solution (75 μL) were prepared and analyzed under the same conditions and at the same time points in order to distinguish between nitroreductase-based activation and enzyme-free hydrolysis. Solutions of sunitinib, erlotinib, and **2b**, prepared as described for the reference measurements, served as standards for the quantification of reaction products.

Biological evaluation

Chemicals for cell culture tests—Erlotinib hydrochloride and sunitinib malate (from LC Laboratories) and all other investigated compounds were dissolved in DMSO. These stock solutions were further diluted in culture media at the indicated concentrations. The final DMSO concentrations were always less than 1%.

Cell culture—The following human cell models were used in this study: the breast carcinoma MCF-7, the colon carcinomas SW480 and HCT116, the renal cell carcinomas Caki-1, Caki-2 and RU-MH, the squamous cell carcinomas H1703 and H520, the epidermoid carcinoma A431, as well as the non-small-cell lung cancer (NSCLC) lines HCC827, PC-9 and Calu3 (sources and used medium are summarized in Table 6). Unless otherwise indicated, the cells were cultivated in humidified incubators (37°C, 21% O_2, 5% CO_2) in full culture medium, containing fetal calf serum (10%, PAA, Linz Austria). Cell cultures were periodically checked for *Mycoplasma* contamination.

Cytotoxicity assay—Cells were plated (2×10^3 cells/well) in 96-well plates and allowed to recover for 24 h. Subsequently, the dissolved drugs were added. After 72 h drug exposure, the proportion of viable cells was determined by MTT assay following the manufacturer's recommendations (EZ4U, Biomedica, Vienna, Austria). Cytotoxicity was expressed as IC_{50} values calculated from full dose-response curves using Graph Pad Prism software.

Hypoxic conditions—Cells were plated in 96- or 6-well plates in a hypoxia chamber (c-chamber equipped with a ProOxC21O_2/CO_2 Controller from Biospherix NY, USA) at 1% O_2/5% CO_2 level for the indicated time points (72 h and 4 h for MTT assays and protein isolation, respectively) before analysis/harvesting. Normoxic sample plates were always prepared in parallel.

Western blot analysis—To assess the impact of our new drugs on the RTK signaling, cells were treated with the test drugs for 4 h. Then, they were harvested, total protein extracts isolated and resolved by SDS-PAGE, and transferred onto a polyvinylidene difluoride membrane for western blotting as previously described.[5c] The antibodies, their source and dilutions are shown in Table 7. Additionally, horseradish-peroxidase-labeled

secondary antibodies from Santa Cruz Biotechnology were used at working dilutions of 1:10 000.

Molecular docking

Molecular docking was performed by the software AutoDock Vina 1.1.2 for Linux[22] using 50 as exhaustiveness value. The Protein Data Bank files PDB ID: 1M17 and PDB ID: 4AGD were used as models for EGFR in complex with erlotinib and VEGFR-2 in complex with sunitinib, respectively. In order to be used for docking studies, the structures of compounds **1a**, **1b**, and **2a–c** were fully optimized by DFT calculations implemented in the Gaussian 09 program package,[23] using the B3LYP functional,[24] and the 6-31G(d) basis set.[25] AutoDock Tools 1.5.6 (cross platform) software was used to add and merge non-polar hydrogens to the receptors and to assign the rotatable bonds to the ligands.[26] The rotational bonds of the proteins were regarded as being rigid. A grid box large enough to allow possible ligand-receptor complexes within the binding pocket of the protein was created (Supporting Information Figure S20). In particular, the grid size for the EGFR receptor was set to 30×20×20 points with grid spacing of 1.000 Å and a grid center of 21.857, 0.260 and 52.761 (center of mass of erlotinib in 1M17), while the grid size for VEGFR-2 receptor was set to 30×30×20 points with grid spacing of 1.000 Å and a grid center of 49.976, −2.120 and −14.836 (center of mass of sunitinib in 4AGD). Validation of AutoDock Vina was performed, running docking calculations on the VEGFR-2 and EGFR receptors and the inhibitors sunitinib and erlotinib as they were in the original PDB (PDB ID: 4AGD and PDB ID: 1M17, respectively). Docking scores of the docked erlotinib and sunitinib, as well as of the docked compounds **1a**, **1b**, and **2a–c**, are reported in Table S1. 2D interactions models were generated using LigPlot + software.[27] Docking results were visualized using Chimera[28] and PyMOL[29] software.

Supplementary Material

Refer to Web version on PubMed Central for supplementary material.

Acknowledgements

We gratefully acknowledge the Initiative Krebsforschung (given to P.H.) and the Austrian Science Fund (FWF), grant P28853 (given to C.R.K.). A.T. received funding from the Mahlke-Obermann Stiftung and the European Union's Seventh Framework Programme for research, technological development, and demonstration under grant agreement no. 609431.

References

[1]. a) Pelengaris S, Khan M, Blasco MA. The Molecular Biology of Cancer. Blackwell; Malden, MA, Oxford: 2006. b) Cheng H, Force T. Prog Cardiovasc Dis. 2010; 53:114–120. [PubMed: 20728698]

[2]. Wu P, Nielsen TE, Clausen MH. Drug Discovery Today. 2016; 21:5–10. [PubMed: 26210956] b)U.S. Department of Health and Human Services: www.fda.gov/Drugs/default.htm (03.05.2016)

[3]. Shah DR, Shah RR, Morganroth J. Drug Safety. 2013; 36:413–426. [PubMed: 23620170]

[4]. a) Coelho SC, Almeida GM, Pereira MC, Santos-Silva F, Coelho MA. Expert Opin Drug Delivery. 2016; 13:133–141.b) Kuruppu AI, Zhang L, Collins H, Turyanska L, Thomas NR, Bradshaw TD. Adv Healthcare Mater. 2015; 4:2816–2821.c) Wan X, Zheng XY, Pang XY, Zhang ZM, Zhang QZ. Colloids Surf B. 2015; 136:817–827.d) Akagi S, Nakamura K, Miura D, Saito Y, Matsubara

Europe PMC Funders Author Manuscripts

H, Ogawa A, Matoba T, Egashira K, Ito H. Int Heart J. 2015; 56:354–359. [PubMed: 25902888] e) Gao HL, Cao SL, Chen C, Cao SJ, Yang Z, Pang ZQ, Xi ZJ, Pan SQ, Zhang QZ, Jiang XG. Nanomedicine. 2013; 8:1429–1442. [PubMed: 23451915]

[5]. a) Blanche EA, Maskell L, Colucci MA, Whatmore JL, Moody CJ. Tetrahedron. 2009; 65:4894–4903.b) Patterson AV, Silva S, Guise C, Bull M, Abbattista M, Hsu A, Sun JD, Hart CP, Pearce TE, Smaill JB. J Clin Oncol. 2015; 33:e13548.c) Karnthaler-Benbakka C, Groza D, Kryeziu K, Pichler V, Roller A, Berger W, Heffeter P, Kowol CR. Angew Chem Int Ed. 2014; 53:12930–12935.Angew Chem. 2014; 126:13144–13149.

[6]. a) Wilson WR, Hay MP. Nat Rev Cancer. 2011; 11:393–410. [PubMed: 21606941] b) Phillips RM. Cancer Chemother Pharmacol. 2016; 77:441–457. [PubMed: 26811177]

[7]. Tatum JL, Kelloff GJ, Gillies RJ, Arbeit JM, Brown JM, Chao KS, Chapman JD, Eckelman WC, Fyles AW, Giaccia AJ, Hill RP, et al. Int J Radiat Biol. 2006; 82:699–757. [PubMed: 17118889]

[8]. Lopci E, Grassi I, Chiti A, Nanni C, Cicoria G, Toschi L, Fonti C, Lodi F, Mattioli S, Fanti S. Am J Nucl Med Mol Imaging. 2014; 4:365–384. [PubMed: 24982822]

[9]. a) Cao J, Campbell J, Liu L, Mason RP, Lippert AR. Anal Chem. 2016; 88:4995–5002. [PubMed: 27054463] b) Li Y, Sun Y, Li J, Su Q, Yuan W, Dai Y, Han C, Wang Q, Feng W, Li F. J Am Chem Soc. 2015; 137:6407–6416. [PubMed: 25923361] c) Bae J, McNamara LE, Nael MA, Mahdi F, Doerksen RJ, Bidwell GL 3rd, Hammer NI, Jo S. Chem Commun. 2015; 51:12787–12790.

[10]. European Commission, Department of Health and Food Safety: ec.europa.eu/health/documents/community-register/html/alfregister.htm (11.05.2016)

[11]. Ferrara N, Davis-Smyth T. Endocr Rev. 1997; 18:4–25. [PubMed: 9034784]

[12]. a) Roskoski R Jr. Pharmacol Res. 2014; 79:34–74. [PubMed: 24269963] b) Brown JM, William WR. Nat Rev Cancer. 2004; 4:437–447. [PubMed: 15170446]

[13]. Rewcastle GW, Denny WA, Bridges AJ, Zhou H, Cody DR, McMichael A, Fry DW. J Med Chem. 1995; 38:3482–3487. [PubMed: 7658435]

[14]. a) Wu P, Nielsen TE, Clausen MH. Trends Pharmacol Sci. 2015; 36:422–439. [PubMed: 25975227] b) Huang Q, Zhou CH, Chen X, Dong B, Chen SQ, Zhang N, Liu YW, Li AR, Yao MC, Miao J, Li Q, et al. PLoS One. 2015; 10:e0141395. [PubMed: 26513662]

[15]. a) Duan JX, Jiao H, Kaizerman J, Stanton T, Evans JW, Lan L, Lorente G, Banica M, Jung D, Wang J, Ma H, et al. J Med Chem. 2008; 51:2412–2420. [PubMed: 18257544] b) Everett SA, Naylor MA, Patel KB, Stratford MRL, Wardman P. Bioorg Med Chem Lett. 1999; 9:1267–1272. [PubMed: 10340612] c)U.S. National Institutes of Health: https://clinicaltrials.gov/ (08.09.2016)

[16]. Tranoy-Opalinski I, Fernandes A, Thomas M, Gesson JP, Papot S. Anti-Cancer Agents Med Chem. 2008; 8:618–637.

[17]. Matteucci M, Duan JX, Jiao H, Kaizerman J, Ammons S. (Threshold Pharmaceuticals Inc.). European Pat. No. EP1896040 A2. 2007.

[18]. a) Williams EM, Little RF, Mowday AM, Rich MH, Chan-Hyams JV, Copp N, Smaill JB, Patterson AV, Ackerley DF. Biochem J. 2015; 471:131–153. [PubMed: 26431849] b) Denny WA. Curr Pharm Des. 2002; 8:1349–1361. [PubMed: 12052212]

[19]. a) Hay MP, Sykes BM, Denny WA, Wilson WR. Bioorg Med Chem Lett. 1999; 9:2237–2242. [PubMed: 10465553] b) Asche C, Dumy P, Carrez D, Croisy A, Demeunynck M. Bioorg Med Chem Lett. 2006; 16:1990–1994. [PubMed: 16442795]

[20]. Juchum M, Gunther M, Laufer SA. Drug Resist Update. 2015; 20:12–28.

[21]. Nurwidya F, Takahashi F, Murakami A, Kobayashi I, Kato M, Shukuya T, Tajima K, Shimada N, Takahashi K. Respir Invest. 2014; 52:82–91.

[22]. Trott O, Olson AJ. J Comput Chem. 2010; 31:455–461. [PubMed: 19499576]

[23]. Frisch MJ, Trucks GW, Schlegel HB, Scuseria GE, Robb MA, Cheeseman JR, Scalmani G, Barone V, Mennucci B, Petersson GA, Nakatsuji H. , et al. Gaussian, Rev 09. Gaussian Inc.; Wallingford, CT (USA); 2009.

[24]. a) Becke AD. J Chem Phys. 1993; 98:5648–5652.b) Lee CT, Yang WT, Parr RG. Phys Rev B. 1988; 37:785–789.c) Stephens PJ, Devlin FJ, Chabalowski CF, Frisch MJ. J Phys Chem. 1994; 98:11623–11627.

[25]. Hariharan PC, Pople JA. Theor Chim Acta. 1973; 28:213–222.

[26]. Morris GM, Huey R, Lindstrom W, Sanner MF, Belew RK, Goodsell DS, Olson AJ. J Comput Chem. 2009; 30:2785–2791. [PubMed: 19399780]

[27]. Laskowski RA, Swindells MB. J Chem Inf Model. 2011; 51:2778–2786. [PubMed: 21919503]

[28]. Pettersen EF, Goddard TD, Huang CC, Couch GS, Greenblatt DM, Meng C, Ferrin TE. J Comput Chem. 2004; 25:1605–1612. [PubMed: 15264254]

[29]. Schrödinger Inc.. PyMOL Molecular Graphics System ver 1.8. Schrödinger LLC; New York, NY (USA): 2015.

Europe PMC Funders Author Manuscripts

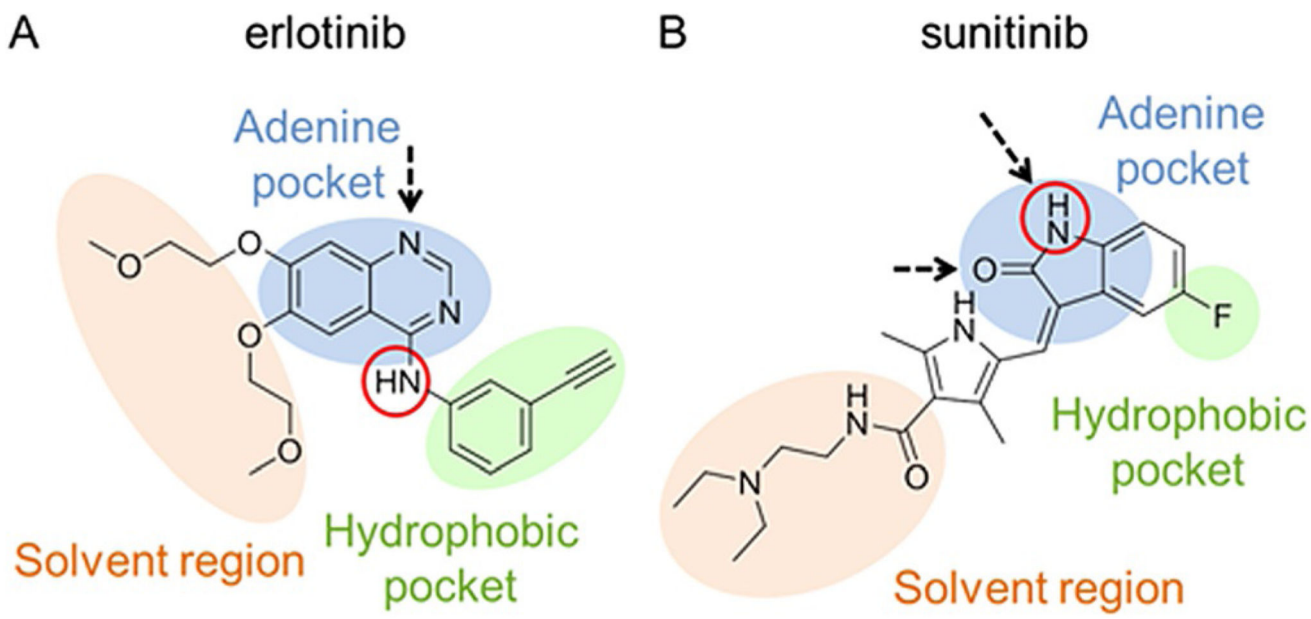

Figure 1.

A) Chemical structure of erlotinib and its schematic binding mode to the EGFR. B) Chemical structure of sunitinib and its schematic binding mode to the VEGFR-2. Hydrogen bonds are indicated by black arrows, nitrogen atoms suitable for derivatization are outlined in red circles. Adapted from Wu et al.[14a]

Europe PMC Funders Author Manuscripts

Europe PMC Funders Author Manuscripts

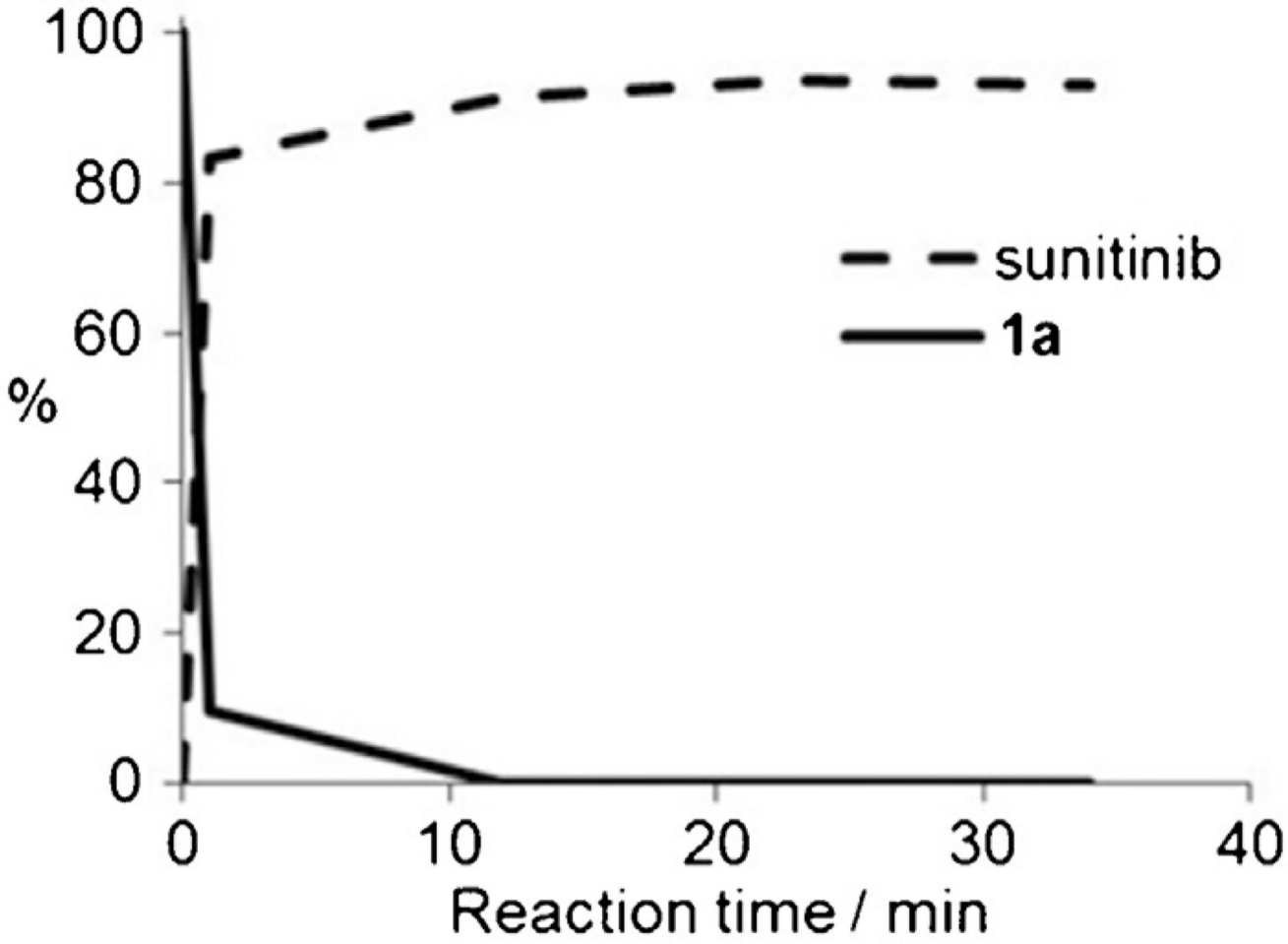

Figure 2.

Release of sunitinib from prodrug **1a** (2.5 μM) upon incubation with NADH (50 μM) and NTR (1.33 μgmL^{-1}) at 37°C. Reactions were followed by HPLC.

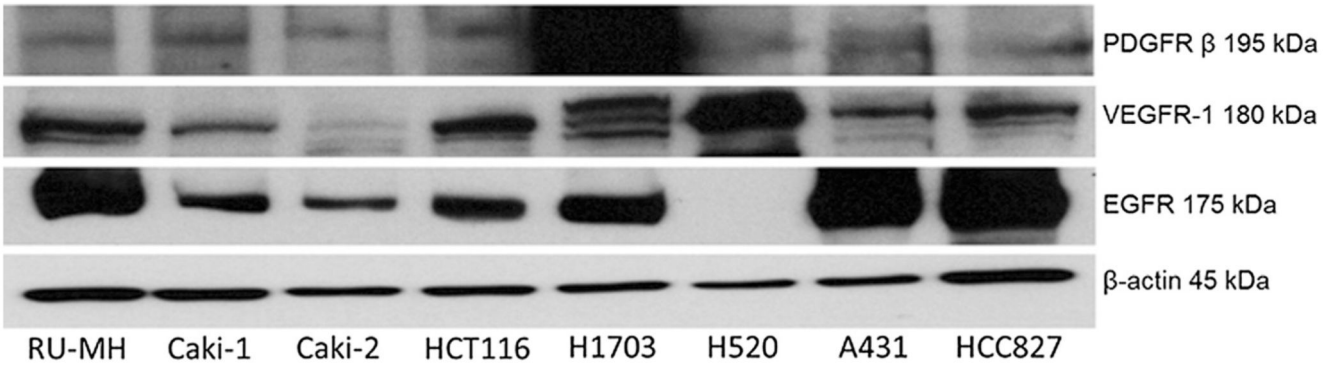

Figure 3.

RTK expression levels of various cancer cell lines. EGFR, PDGFRβ, and VEGFR-1 expression of the indicated cell lines were measured in membrane-enriched fractions by western blot. β-Actin expression served as loading control.

Europe PMC Funders Author Manuscripts

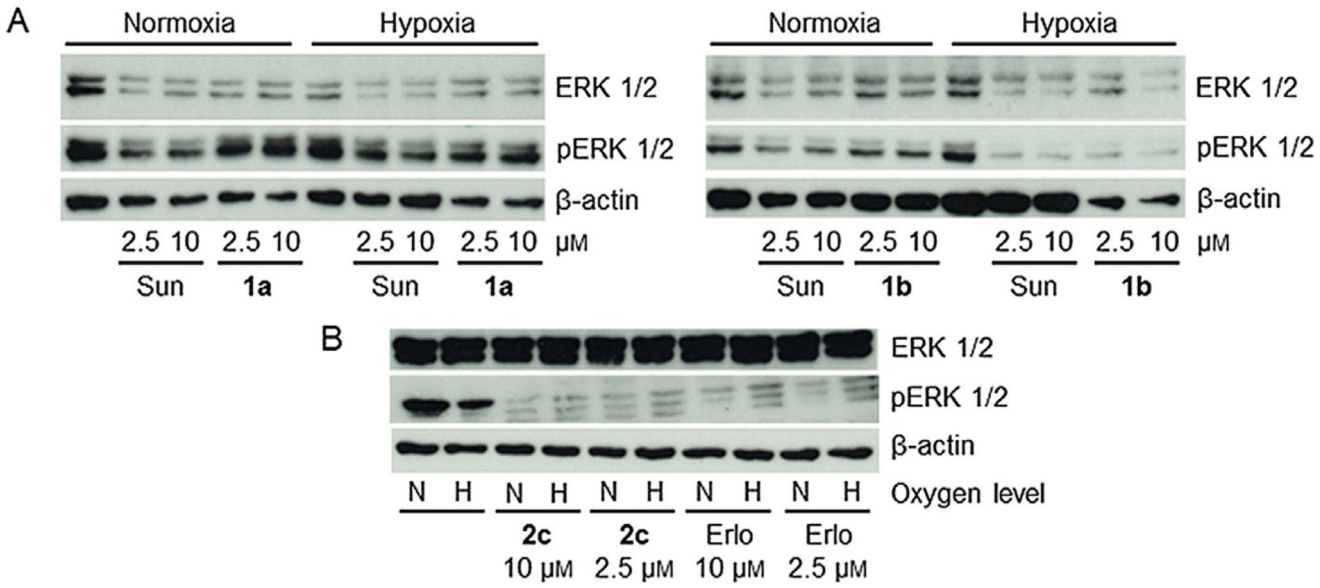

Figure 4.

Inhibitory effects of the novel prodrugs in comparison with the respective free TKI on RTK signaling. A) Sunitinib-sensitive A431 and B) erlotinib-hypersensitive PC-9 cells were grown in medium with fetal calf serum (FCS) and treated with the indicated drug for 4 h. They were then harvested and lysed, and the impact on ERK phosphorylation as a read out for RTK signaling was analyzed by western blotting. Sun = sunitinib, Erlo = erlotinib, N = normoxia, H = hypoxia.

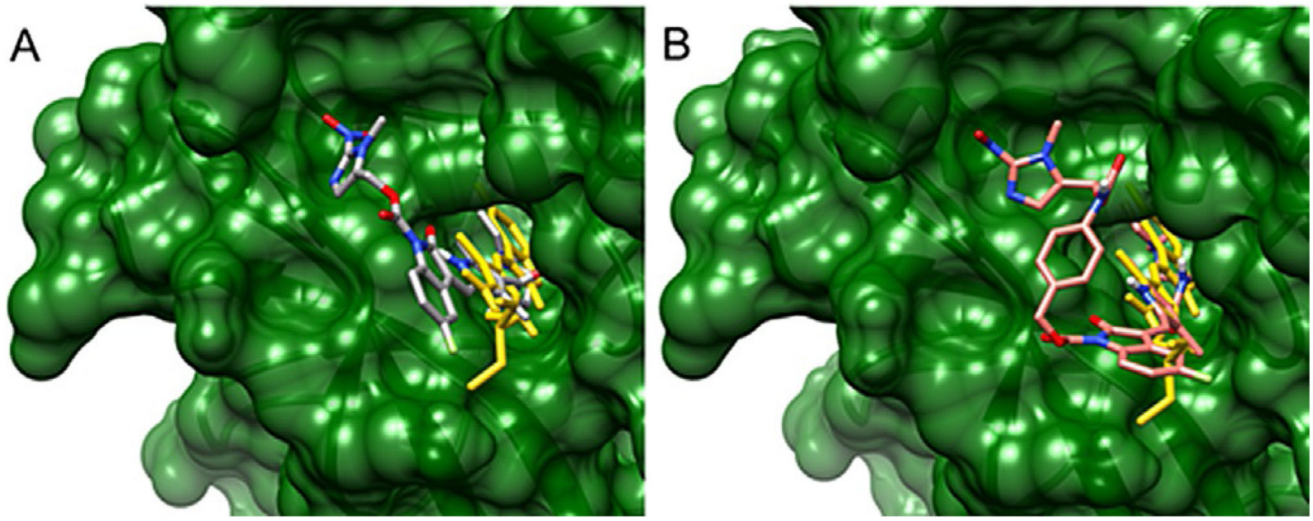

Figure 5.

3D structures of A) sunitinib and compound **1a**, and B) sunitinib and **1b** in complex with VEGFR-2. The structure of the VEGFR-2–sunitinib complex was obtained from PDB ID: 4AGD. The protein is depicted in ribbon representation colored in green and was rendered as a surface representation. Pictures were generated using Chimera. Compounds are shown in capped stick representation and colored as follows: A) sunitinib in gold, **1a** in dark grey; B) sunitinib in gold, **1b** in red/salmon. For both derivatives, the oxindole core is clearly outside the protein binding pocket.

Europe PMC Funders Author Manuscripts

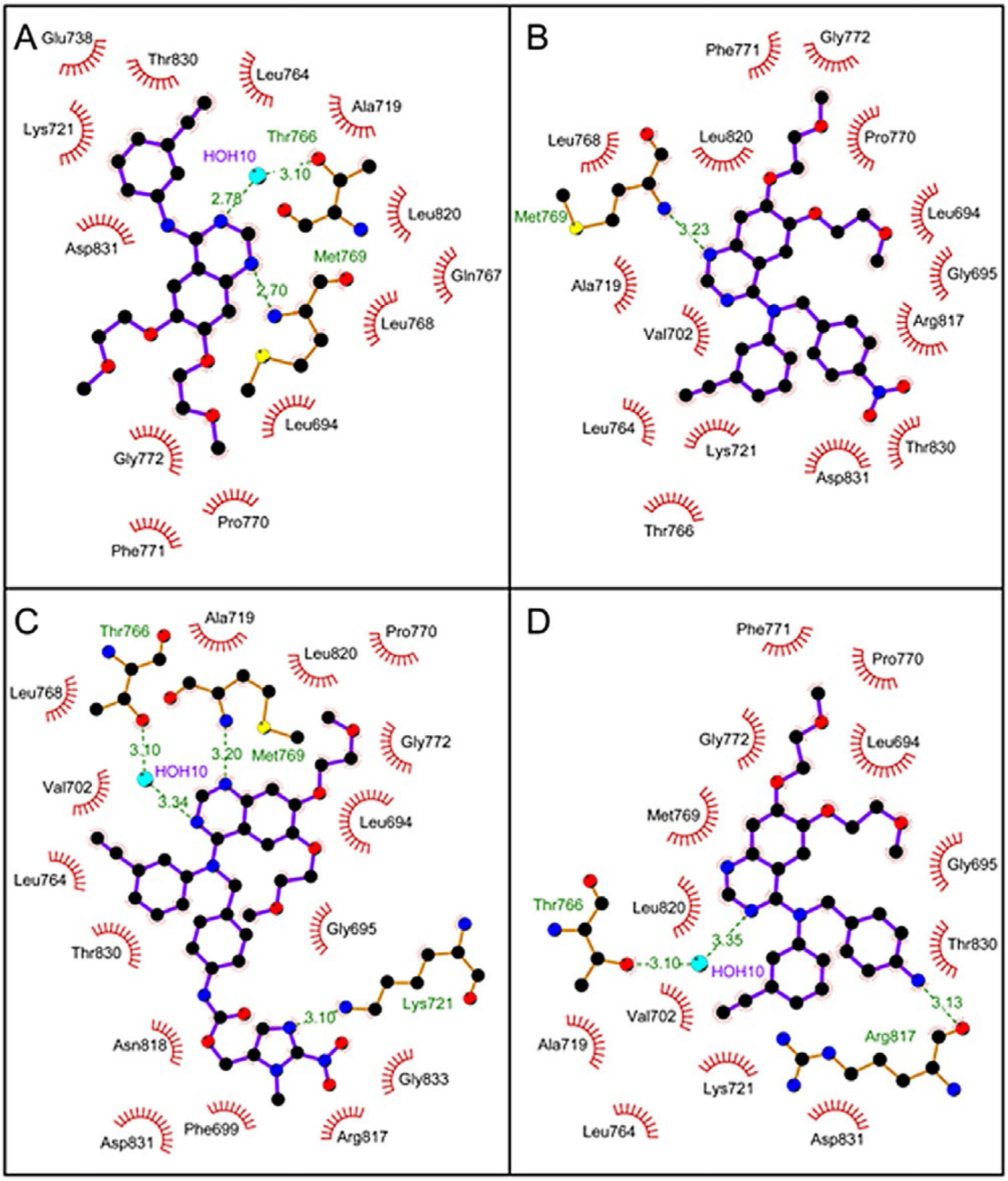

Figure 6.

Schematic 2D diagrams of protein–ligand interactions for EGFR in complex with A) erlotinib (PDB ID: 1M17), B) **2a**, C) **2c**, and D) **2b**. Hydrogen bonds are indicated by dashed lines, while hydrophobic contacts are represented by an arc with spokes radiating toward the ligand atoms they contact. The contacted atoms are shown with spokes radiating back.

Europe PMC Funders Author Manuscripts

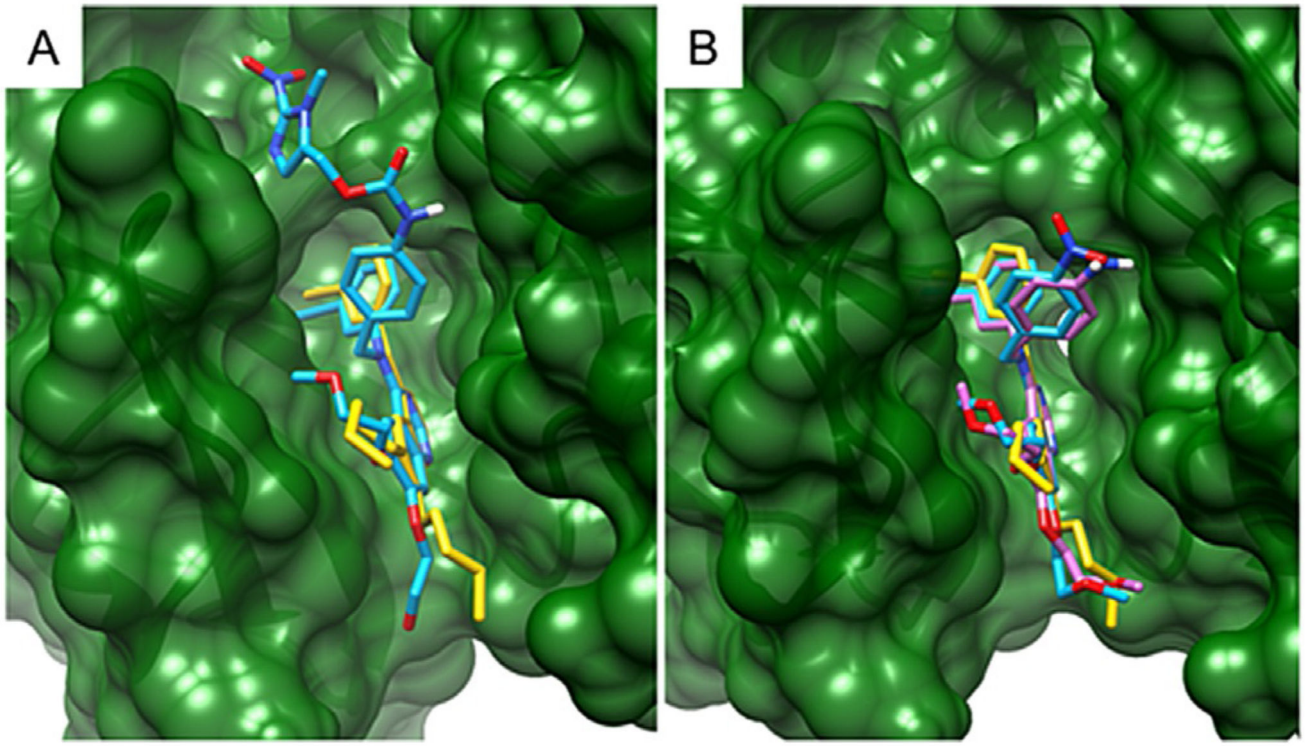

Figure 7.

3D structures of A) erlotinib and compound **2c**, and B) erlotinib, **2a** and **2b** in complex with EGFR. The structure of the EGFR–erlotinib complex was obtained from PDB ID: 1M17. The protein is depicted in ribbon representation colored in green and was rendered as a surface representation. Compounds are shown in capped stick representation and colored as follows: A) erlotinib in gold, **2c** in sky blue; B) erlotinib in gold, **2a** in sky blue and **2b** in magenta. The pictures were generated using Chimera.

Europe PMC Funders Author Manuscripts

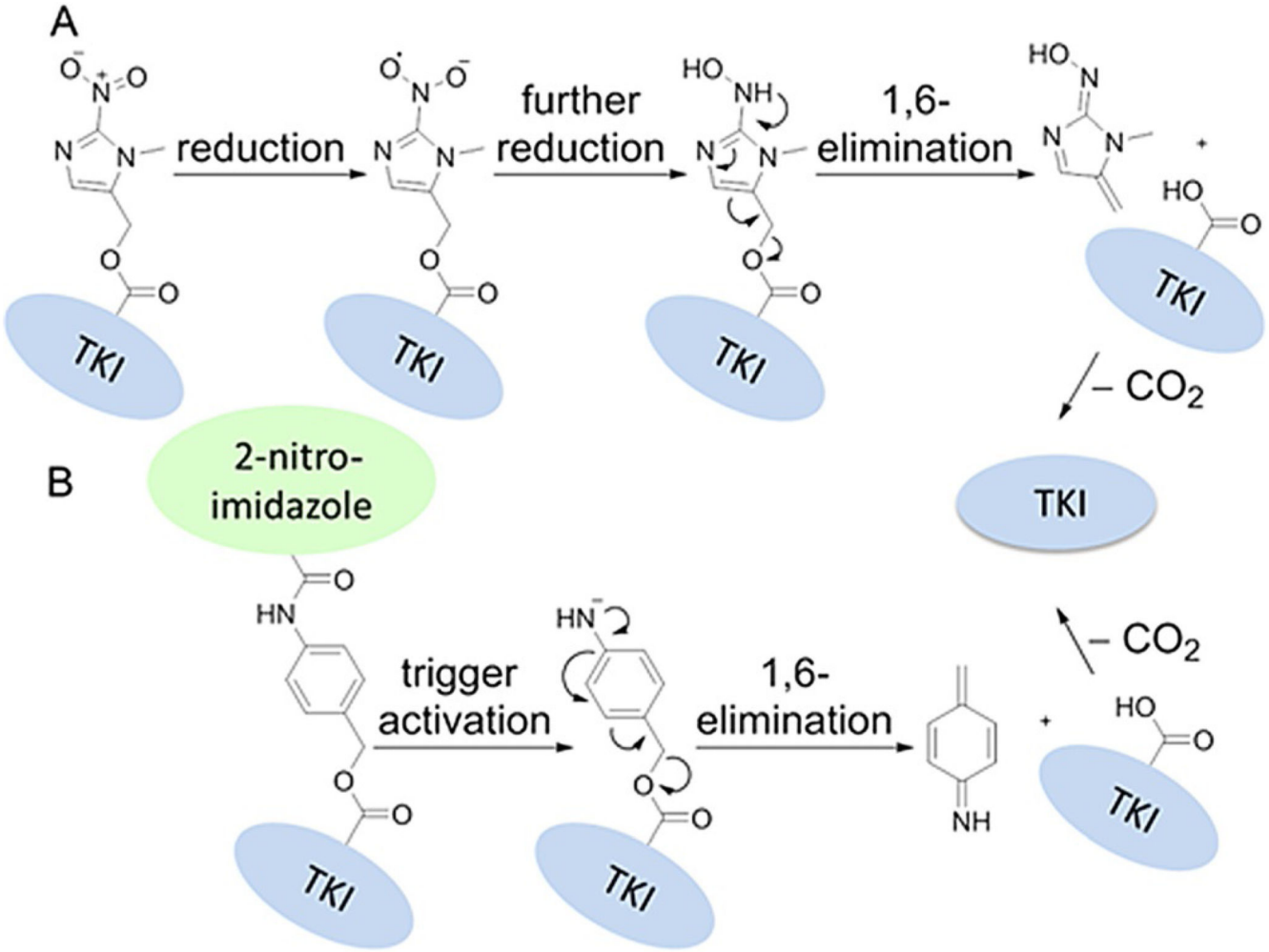

Scheme 1.

Postulated schematic pathway of TKI release for A) two-part compounds upon trigger reduction, and B) three-part compounds upon trigger reduction and linker decomposition.

Europe PMC Funders Author Manuscripts

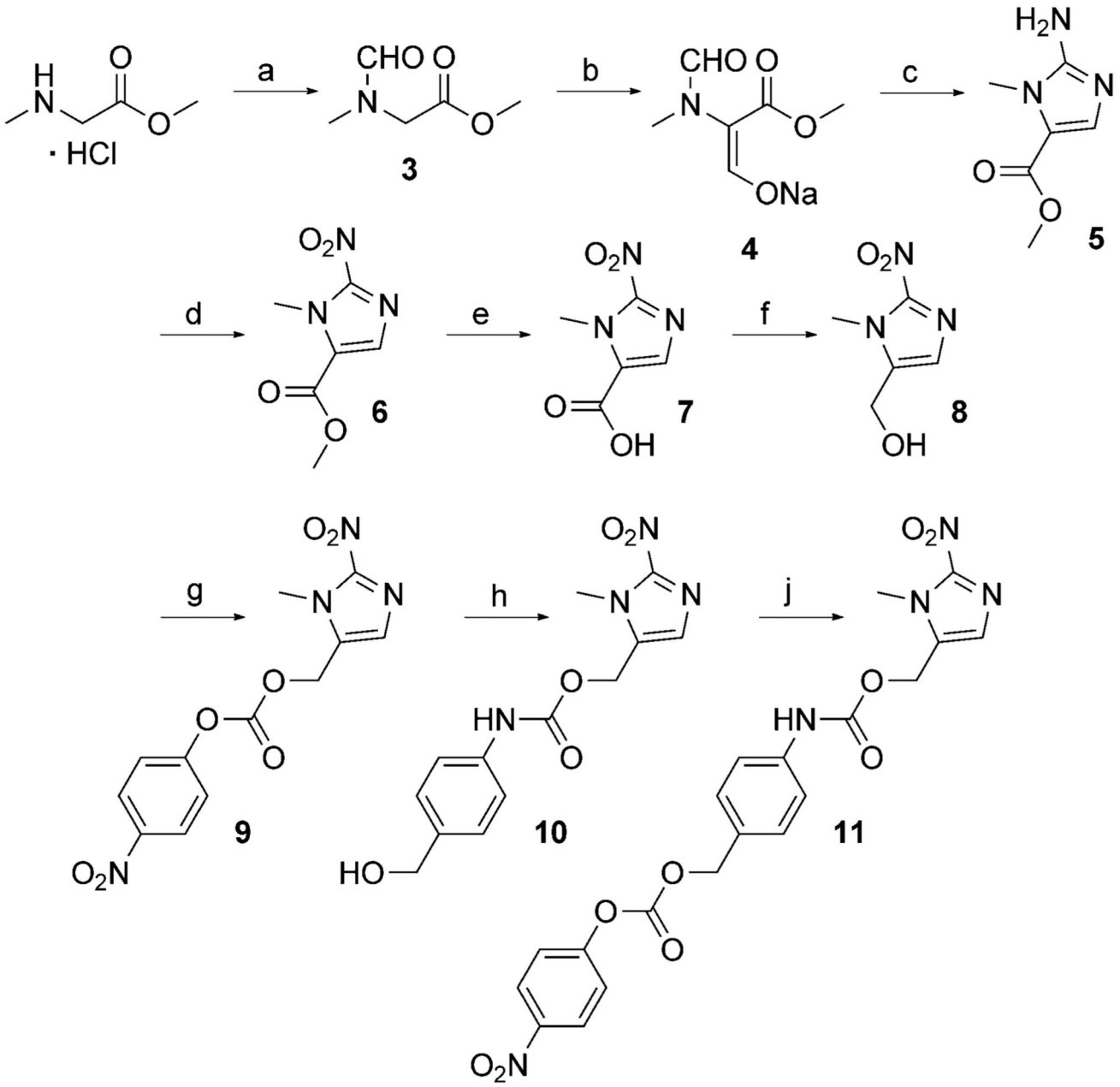

Scheme 2.

Synthetic route of 1-methyl-2-nitro-1*H*-imidazole-5-methanol (**8**), and the conjugation substrates **9** and **11**. *Reagents and conditions*: a) HCO_2Me, K_2CO_3, MeOH; b) HCO_2Me, NaOMe, THF abs.; c) 1. HCl, MeOH, 2. NH_2CN, NaOAc; d) $NaNO_2$, HOAc, H_2O; e) NaOH (1 M), H_2O; f) 1. isobutyl chloroformate, Et_3N, THF abs., 2. $NaBH_4$, H_2O; g) 4-nitrophenyl chloroformate, pyridine, THF abs.; h) 4-aminobenzyl alcohol, HOBt·H_2O, DMF abs.; j) bis(4-nitrophenyl) carbonate, DIPEA, DMF abs.

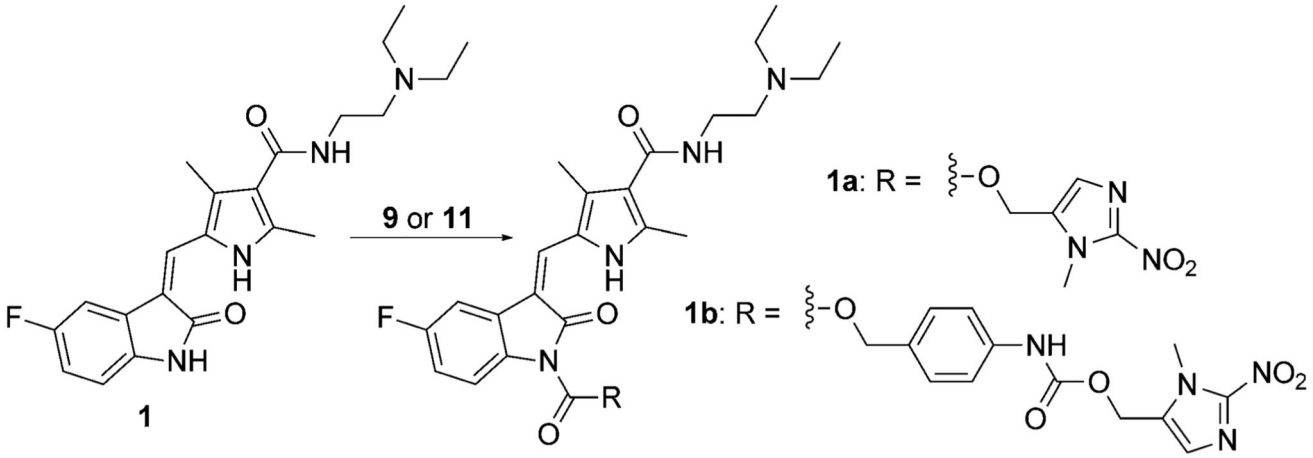

Scheme 3.

Synthesis of sunitinib prodrugs **1a** and **1b**. *Reagents and conditions*: **9** or **11**, 4-DMAP, THF abs., 68 h.

Europe PMC Funders Author Manuscripts

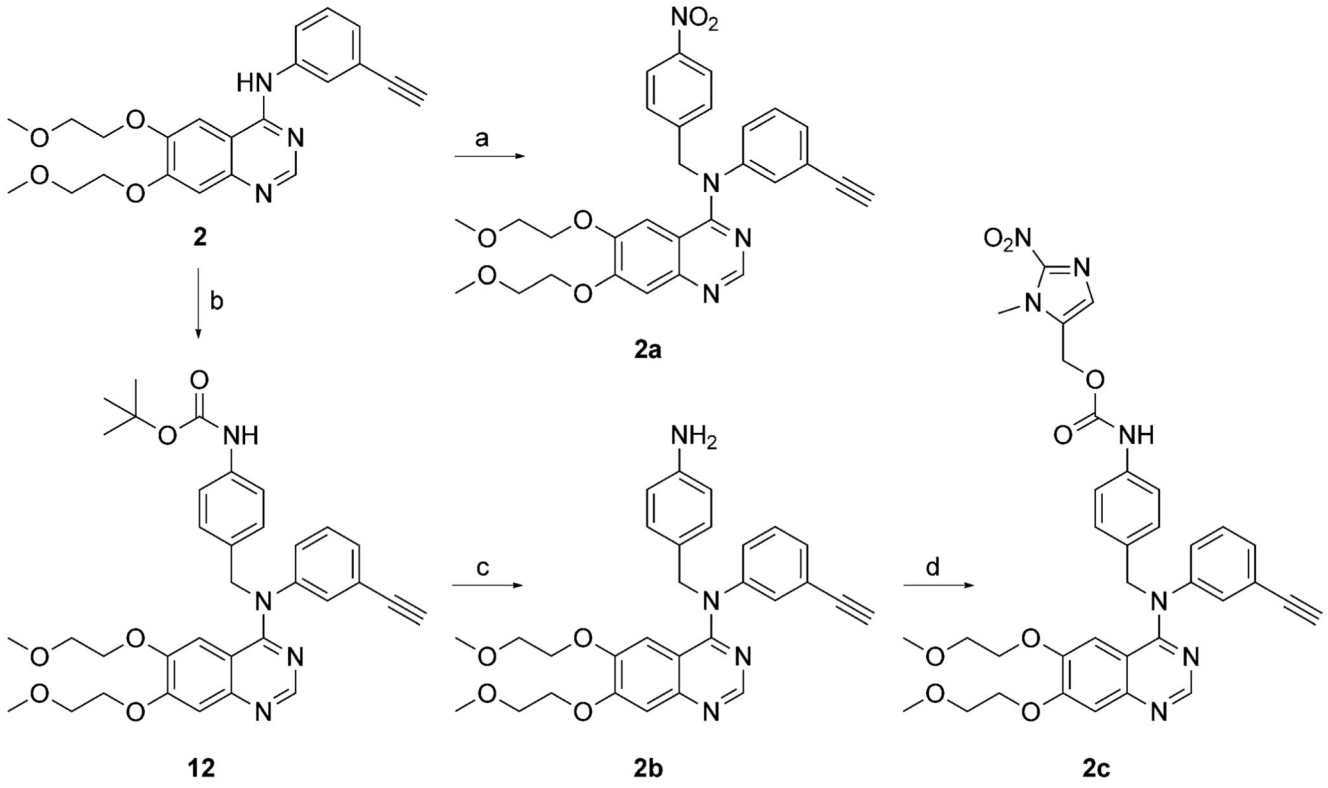

Scheme 4.

Synthesis of erlotinib prodrugs **2a** and **2c**. *Reagents and conditions*: a) 4-nitrobenzyl bromide, *t*BuOK, DMF abs.; b) Boc-4-aminobenzyl bromide, *t*BuOK, DMF abs.; c) HCl conc., MeOH; d) **9**, HOBt·H_2O, DMF abs.

Europe PMC Funders Author Manuscripts

Europe PMC Funders Author Manuscripts

Table 1

Stability and NTR activation of compounds **1a**, **1b**, and **2a–2c**.

Compd	Stability [%][a]	NTR activation[b]		
		$t_{1/2}$ [min]	Amount of substrate after 15 min [%]	Product and amount after 25 min
1a	14	<1	0	sunitinib, 93%
1b	4	<6	10	sunitinib, 58%
2a	88	<6	10	erlotinib, 44%
2b	90	–	100	–
2c	76	<6	0	**2b**, 90%

[a]Aqueous stability of compound solutions (2.5 μM) after 24 h in phosphate buffer (10 mM, pH 7.4, 37°C), determined by HPLC.

[b]Reduction and subsequent fragmentation of compounds (2.5 μM) in phosphate-buffered solutions by incubation with NADH (50 μM) and NTR (1.33 μg mL^{-1}) at 37°C, calculated from the HPLC chromatogram peak areas as a function of time.

Europe PMC Funders Author Manuscripts

Table 2

IC_{50} values of sunitinib and erlotinib against the indicated cell lines after 72 h of treatment.

Cell line	IC_{50} [μM][a]	
	Sunitinib	Erlotinib
RU-MH	6.6 ± 1.3	23.0 ± 2.6
Caki-1	6.8 ± 0.2	n.t.
Caki-2	> 10	n.t.
HCT116	4.6 ± 0.3	> 25
H1703	0.5 ± 0.0	n.t.
A431	7.3 ± 0.4	7.6 ± 1.7
HCC827	5.2 ± 0.5	0.3 ± 0.2
H520	4.2 ± 0.4	> 25
SW480	n.t.	> 25
MCF-7	n.t.	> 25
Calu3	9.6 ± 0.1	2.0 ± 0.5
PC-9	n.t.	1.4 ± 0.8

[a]Values are the mean ± SD of $n = 3$ experiments performed in triplicate; n.t.: not tested.

Table 3

IC_{50} values of sunitinib, **1a**, and **1b** against the indicated cell lines under normoxia vs. hypoxia after 72 h of treatment.

Cell line	Sunitinib			1a			1b		
	IC_{50} [μM][a]		fold diff.	IC_{50} [μM][a]		fold diff.	IC_{50} [μM][a]		fold diff.
	N	H		N	H		N	H	
A431	5.9 ± 1.4	4.2 ± 0.6	1.4	6.8 ± 0.3	4.4 ± 0.1	1.5	6.7 ± 0.5	4.5 ± 0.5	1.5
Caki-1	6.8 ± 0.2	7.6 ± 1.4	0.9	6.6 ± 0.4	6.6 ± 0.5	1.0	5.5 ± 1.4	5.6 ± 1.2	1.0
HCC827	5.2 ± 0.5	3.4 ± 0.1	1.4	5.5 ± 1.0	3.5 ± 0.3	1.6	5.5 ± 1.7	3.9 ± 1.2	1.4
HCT116	2.2 ± 1.5	2.0 ± 1.2	1.1	2.1 ± 1.7	2.2 ± 1.3	1.0	1.9 ± 1.3	2.1 ± 1.3	0.9
H1703	0.5 ± 0.0	0.5 ± 0.0	1.0	0.5 ± 0.0	0.5 ± 0.0	1.0	0.5 ± 0.0	0.5 ± 0.0	1.0

[a]Values are the mean ± SD of $n = 3$ experiments performed in triplicate; N: normoxia, H: hypoxia.

Table 4

IC_{50} values of **2a**, **2b**, and **2c** against the indicated cell lines under normoxia vs. hypoxia after 72 h of treatment.

Cell line	2a			2b			2c		
	IC_{50} [μM][a]		fold diff.	IC_{50} [μM][a]		fold diff.	IC_{50} [μM][a]		fold diff.
	N	H		N	H		N	H	
A431	15.0 ± 3.5	16.7 ± 2.8	1.1	> 25	> 25	1.0	3.8 ± 2.5	2.5 ± 1.4	1.5
HCC827	2.7 ± 1.4	1.9 ± 0.9	1.4	2.7 ± 0.9	1.8 ± 0.3	1.5	2.6 ± 1.0	2.1 ± 1.1	1.2
PC-9	7.5 ± 1.0	7.0 ± 0.9	1.1	6.8 ± 2.1	3.2 ± 0.1	2.1	6.0 ± 2.8	3.0 ± 0.8	2.0
Calu3	15.5 ± 1.3	15.5 ± 3.4	1.0	> 25	14.9	> 1.7	5.8 ± 3.7	5.0 ± 3.8	1.2
SW480	> 25	> 25	1.0	> 25	> 25	1.0	2.4 ± 1.5	1.8 ± 1.1	1.3
MCF-7	9.0 ± 1.0	12.4 ± 2.8	0.8	> 25	> 25	1.0	0.6 ± 0.0	0.7 ± 0.1	0.9

[a]Values are the mean ± SD of $n = 3$ experiments performed in triplicate; N: normoxia, H: hypoxia.

Table 5

IC_{50} values of erlotinib and TH-302 against the indicated cell lines under normoxia vs. hypoxia after 72 h of treatment.

Cell line	Erlotinib			TH-302		
	IC_{50} [μM][a]		fold diff.	IC_{50} [μM][a]		fold diff.
	N	H		N	H	
A431	7.6 ± 1.7	9.9 ± 2.9	0.8	22.4 ± 2.6	5.4 ± 3.4	4.1
HCC827	0.3 ± 0.2	0.3 ± 0.2	1.0	> 10	7.4 ± 0.0	> 1.4
PC-9	1.4 ± 0.8	1.3 ± 0.9	1.1	10.0 ± 0.0	5.9 ± 4.1	1.7
Calu3	2.0 ± 0.5	1.3 ± 0.4	1.5	17.5 ± 7.5	6.3 ± 3.7	2.8
SW480	> 25	> 25	1.0	20.6 ± 5.9	8.3 ± 2.9	2.5
MCF-7	> 25	> 25	1.0	22.5 ± 2.5	2.2 ± 0.4	10.2

[a]Values are the mean ± SD of $n = 3$ experiments performed in triplicate; N: normoxia, H: hypoxia.

Europe PMC Funders Author Manuscripts

Table 6

Detailed information on the cell lines used.[a]

Cell line	Histology	Characteristics	Growth medium	Source
A431	Epidermoid carcinoma	EGFR wild-type overexpression, erlotinib-sensitive	RPMI-1640	ATCC
Caki-1	Renal cell carcinoma		McCoy's	ATCC
Caki-2	Renal cell carcinoma		McCoy's	ATCC
Calu3	NSCLC	EGFR-dependent, erlotinib-sensitive	MNP	ATCC
HCC827	NSCLC	Erlotinib-sensitive due to EGFR mutation (delE746–A750)	RPMI-1640	ATCC
MCF-7	Mammary tumor, adenocarcinoma		DMEM	ATCC
PC-9	NSCLC	Erlotinib-sensitive due to EGFR mutation (delE746–A750)	RPMI-1640	CEMM–Kilian Huber
RU-MH	Renal cell carcinoma		RPMI-1640	Established at the ICR
HCT116	Colorectal carcinoma	EGFR wild-type	McCoy's	ATCC
SW480	Colorectal carcinoma	EGFR wild-type	MEME	ATCC
H1703	Squamous cell lung carcinoma		RPMI-1640	ATCC
H520	Squamous cell lung carcinoma		RPMI-1640	ATCC

[a]Abbreviations: ATCC, American Type Culture Collection; DMEM, Dulbecco's modified Eagle's medium; ICR, Institute of Cancer Research Vienna; MNP, minimal essential medium with non-essential amino acids and pyruvate.

Europe PMC Funders Author Manuscripts

Table 7

Antibodies used.

Primary antibody	Specification	Dilution	Source
β-actin	Monoclonal mouse	1:5000	Sigma–Aldrich
EGFR	Monoclonal rabbit	1:1000	Cell Signaling
VEGFR-1	Polyclonal rabbit	1:1000	Cell Signaling
PDGFRβ	Monoclonal rabbit	1:1000	Cell Signaling
ERK1/2 (p44/42 MAPK)	Polyclonal rabbit	1:1000	Cell Signaling
pERK (Thr202/Tyr204)	Polyclonal rabbit	1:1000	Cell Signaling